Iron-sulfur cluster loss in mitochondrial CISD1 mediates PINK1 loss-of-function phenotypes

Sara Bitar[1], Timo Baumann[1], Christopher Weber[1], Majd Abusaada[1], Liliana Rojas-Charry[1], Patrick Ziegler[2], Thomas Schettgen[2], Isabella Eva Randerath[2], Vivek Venkataramani[3], Bernhard Michalke[4], Giuseppe Arena[3], Rejko Krüger[3, 4, 5], Li Zhang[1#], and Axel Methner[1#]

Running title: CISD PD

[1]University Medical Center of the Johannes Gutenberg-University Mainz, Institute for Molecular Medicine, Langenbeckstr. 1, D-55131 Mainz, Germany.

[2]Institute for Occupational, Social and Environmental Medicine, Medical Faculty, RWTH Aachen University, Pauwelsstrasse 30, 52074 Aachen, Germany.

[3]Comprehensive Cancer Center Mainfranken, University Hospital Würzburg, 97080 Würzburg, Germany.

[4]Research Unit Analytical BioGeoChemistry, Helmholtz Zentrum München-German Research Center for Environmental Health GmbH, 85764 Neuherberg, Germany.

[3]University of Luxembourg, Luxembourg Centre for Systems Biomedicine, 6, Avenue du Swing, L-4367 Esch-sur-Alzette, Luxembourg.

[4]Luxembourg Institute of Health (LIH), 1A-B, rue Thomas Edison,, L-1445 Strassen

[5]Centre Hospitalier de Luxembourg (CHL), 4, Rue Nicolas Ernest Barblé, 1210 Luxembourg

Correspondence should be addressed to Li Zhang, PhD lizhang2017deu@gmail.com or Axel Methner, MD axel.methner@gmail.com,

Abstract

Parkinson's disease (PD) is characterized by the progressive loss of dopaminergic neurons in the substantia nigra of the midbrain. Familial cases of PD are often caused by mutations of PTEN-induced kinase 1 (PINK1) and the ubiquitin ligase Parkin, both pivotal in maintaining mitochondrial quality control. CISD1, a homodimeric mitochondrial iron-sulfur-binding protein, is a major target of Parkin-mediated ubiquitination. We here discovered a heightened propensity of CISD1 to form dimers in *Pink1* mutant flies and in dopaminergic neurons from PINK1 mutation patients caused by loss of its iron-sulfur cluster. Reintroducing a CISD1 mutant incapable of binding the iron-sulfur cluster into CISD1 knockout cells failed to rescue mitochondrial fragmentation and oxidative distress. When overexpressed in Drosophila, this mutant proved detrimental by disrupting the redox equilibrium. Complete loss of *Cisd*, the Drosophila orthologue of CISD1, rescued all detrimental effects of Pink1 mutation on climbing ability, wing posture, dopamine levels, lifespan, and mitochondrial ultrastructure. Our results suggest that Cisd, probably iron-depleted Cisd, operates downstream of Pink1 shedding light on PD pathophysiology and implicating CISD1 as a potential therapeutic target.

Introduction

Parkinson's disease (PD) is the fastest growing neurodegenerative disorder clinically characterized by rigor, tremor and bradykinesia. These motor symptoms stem from the progressive degeneration of dopaminergic neurons in the midbrain's substantia nigra pars compacta (reviewed in (Pickrell & Youle, 2015)). While most cases are sporadic, familial forms of PD are linked to mutations in genes that encode proteins involved in mitochondrial quality control like PTEN-induced kinase 1 (PINK1) and Parkin (PRKN), providing valuable insights into the pathophysiology of PD (Shulman *et al*, 2011). In healthy cells, PINK1 is continuously imported into mitochondria, where it is rapidly degraded (Narendra *et al*, 2008). However, in unfit mitochondria with a reduced mitochondrial membrane potential ($\Delta\psi_m$), PINK1 import stalls. When PINK1 accumulates on damaged mitochondria, it phosphorylates various proteins, including the E3 ubiquitin ligase PRKN. This phosphorylation activates PRKN, enabling it to attach ubiquitin to mitochondrial proteins. This ubiquitination acts as a signal for damaged mitochondria to be identified and engulfed by autophagosomes, initiating their degradation through mitophagy. This selective elimination of compromised mitochondria safeguards overall mitochondrial health and function (reviewed in (Youle & Narendra, 2011)). Much of this mechanistic understanding has been elucidated in the fruit fly *Drosophila melanogaster* where *Pink1* and *Prkn* loss of function results in profound changes of the mitochondrial ultrastructure causing mitochondrial dysfunction, impaired flight and climbing ability, and a shortened lifespan (Clark *et al*, 2006; Park *et al*, 2006).

In addition to disturbances in mitochondrial quality control, disruptions in iron metabolism contribute significantly to the pathogenesis of PD (Ma *et al*, 2021). PD patients exhibit elevated iron levels within the substantia nigra pars compacta, and this iron accumulation correlates with the severity of the disease (Dexter *et al*, 1987; Hirsch *et al*, 1991). Notably, this iron dysregulation is apparent even in asymptomatic carriers of *PRKN* mutations (Pyatigorskaya *et al*, 2015), suggesting that it is an early event and correlated with mitochondrial dysfunction. Furthermore, human dopaminergic neurons lacking PINK1 display inhibition of the iron-dependent mitochondrial aconitase, leading to accumulation of NAD^+ and depletion of essential metabolites (Bus *et al*, 2020). In flies, *Pink1* deficiency similarly results in inactivation of mitochondrial aconitase by impairing its labile iron-sulfur cluster, leading to oxidative distress and mitochondrial swelling (Esposito *et al*, 2013; Wan *et al*, 2020). These findings highlight the relevance of iron dysregulation in the PD development and progression.

An important target protein of PINK1/PRKN crucial for iron homeostasis and redox homeostasis is CISD1, also known as mitoNEET (reviewed in (Mittler *et al*, 2019)). CISD1 is a homodimeric protein N-terminally inserted into the outer mitochondrial membrane facing the cytosol (Wiley *et al*, 2007a). CISD1 is ubiquitinated by PRKN (Sarraf *et al*, 2013) and its levels are reduced upon dissipation of $\Delta\psi_m$ (Chan *et al*, 2011; Narendra *et al*, 2012; Okatsu *et al*, 2012; McWilliams *et al*, 2018; Cunningham *et al*, 2015; Lazarou *et al*, 2013). Moreover, CISD1 forms a complex with PRKN, and this interaction is markedly increased by activation of PINK1 and ubiquitination (Sarraf *et al*, 2013; Narendra *et al*, 2013). In *Drosophila*, the homolog of CISD1 is the most strongly ubiquitinated protein in response to Prkn overexpression in vivo (Martinez *et al*, 2017).

Functionally, CISD1 exists as a homodimer, and each monomer of CISD1 harbors a 2Fe/2S (2 iron / 2 sulfur) cluster coordinated by three cysteines and one histidine. In contrast, most conventional 2Fe/2S clusters are coordinated by four cysteines or two cysteines and two histidines (Wiley *et al*, 2007b). This peculiarity renders the CISD1 2Fe/2S cluster more

susceptible to oxidation. It was thus proposed that the transfer of the iron-sulfur cluster from CISD1 to stress-sensitive Fe-S proteins constitutes a cellular adaptive response that helps recovery from oxidative injury ((reviewed in (Mittler *et al*, 2019)). In support of this hypothesis, it has been demonstrated that the oxidized 2Fe/2S cluster of CISD1 can be transferred to iron regulatory protein 1 (IRP1) (Ferecatu *et al*, 2014), a bifunctional protein that can switch between two distinct enzymatic activities based on the availability of iron. When iron levels are sufficient, IRP1 binds an 2Fe/2S cluster, converting it into a functional aconitase enzyme. When iron levels are low, IRP1 loses its 2Fe/2S cluster and undergoes a conformational change. In this state, known as the "apo" form, IRP1 functions as an RNA-binding protein and binds to specific RNA sequences called iron-responsive elements (IREs) located in the untranslated regions of target mRNAs (reviewed by (Rouault & Maio, 2017)). CISD1 is capable of recycling the cytosolic apo-IRP1 to holo-aconitase by donating its 2Fe/2S cluster (Camponeschi *et al*, 2017). The fate of the remaining apo-CISD1 is unknown. In addition to its role in iron metabolism and defense against oxidative stress, CISD1 is also involved in mitochondrial bioenergetics and in the regulation of mitochondrial morphology. Cardiac myocytes from *Cisd1* knockout (KO) mice exhibit a reduced mitochondrial oxidative capacity (Wiley *et al*, 2007a), akin to KO mouse embryonic fibroblasts (MEFs) where this dysfunction is attributed to a reduction in the total cellular mitochondrial volume (Vernay *et al*, 2017).

In Drosophila, there is a single orthologue of CISD1 initially named Cisd2 because it is slightly more similar to the mammalian CISD2 than to CISD1 (Jones *et al*, 2014) protein. Human CISD2 is located at the membrane of the endoplasmic reticulum (Wang *et al*, 2014). Overexpression of Cisd2 (this publication used the alternative name Dosmit) in fly muscles is detrimental and results in mitochondrial enlargement and the formation of double-membraned vesicles containing cytosolic protein within mitochondria (Chen *et al*, 2020), implicating Cisd2 in the regulation of mitochondrial morphology. Similar to human CISD1, fly Cisd2 (this publication used the alternative name MitoNEET) interacts with IRP1 (Huynh *et al*, 2019) further linking Cisd2 to iron homeostasis. Together these findings suggest that fly Cisd2 rather resembles the human mitochondrial homolog CISD1 and to avoid confusion, we will henceforth use Cisd for the fly orthologue. Based on the involvement of CISD1 in mitochondrial bioenergetics and quality control, defense against oxidative stress and iron metabolism – all hallmarks of PD – we aimed to investigate CISD1's role in PD using fly and mammalian model systems.

In our study, we have identified CISD1, particularly its iron-depleted apo form, as a downstream mediator of the pathology resulting from the loss of Pink1 and Prkn function. Apo-CISD1 accumulates in PINK1 patient-derived human dopaminergic neurons and apo-Cisd in mutant *Pink1* flies. Complete loss of *Cisd* rescues all detrimental effects of *Pink1* loss of function on climbing ability, wing posture, dopamine levels, lifespan, and mitochondrial ultrastructure. In *Prkn* mutant flies, *Cisd* deficiency ameliorates climbing ability and wing posture impairments, but does not mitigate the reduction in lifespan. These findings strongly suggest that the buildup of iron-depleted CISD1 may contribute to the pathophysiology of both familial and sporadic Parkinson's disease.

Results

Increased CISD1 dimer formation in human dopaminergic neurons from PD patients with a PINK1 Q456X mutation

To investigate a possible involvement of CISD1 and its homolog CISD2 in familial Parkinson's disease, we studied their expression levels in differentiated dopaminergic

neurons from two distinct patients afflicted with autosomal-recessive PD caused by *PINK1* Q456X mutation. This specific mutation introduces a premature stop codon, leading to increased apoptosis of tyrosine hydroxylase-positive dopaminergic neurons, accompanied by increased levels of alpha-synuclein in the surviving dopaminergic neurons and astrogliosis (Jarazo *et al*, 2022). Both *PINK1* mutant and gene-corrected induced-pluripotent stem cells were first converted into neuroepithelial stem cells and then further differentiated into midbrain-specific dopaminergic neurons as previously described (Reinhardt *et al*, 2013). Notably, *PINK1* Q456X neurons expressed diminished *PINK1* mRNA levels (Figure 1A) and reduced levels of tyrosine hydroxylase (as depicted in exemplary blots from our differentiations in Figure 1B, with quantification of different differentiations reported in Jarazo et. al. (Jarazo *et al*, 2022)). We then employed immunoblotting to concurrently assess the abundance of both mitochondrial CISD1 and endoplasmic reticulum CISD2 proteins, because both proteins are recognized by our antibody (Wang *et al*, 2014; Martinez *et al*, 2023). The ability of this antibody to identify both homologs was previously demonstrated by subcellular fractionation (Wang *et al*, 2014) and specific siRNA-mediated knockdown of either *CISD1* or *CISD2* (Martinez *et al*, 2023). It is also noteworthy that both proteins form homodimers with high stringency even on reducing gels (Antico *et al*, 2021; Paddock *et al*, 2007). *Cisd1* KO and wildtype (WT) mouse embryonic fibroblasts (Vernay *et al*, 2017) served to identify the correct bands (Figure 1C/C').

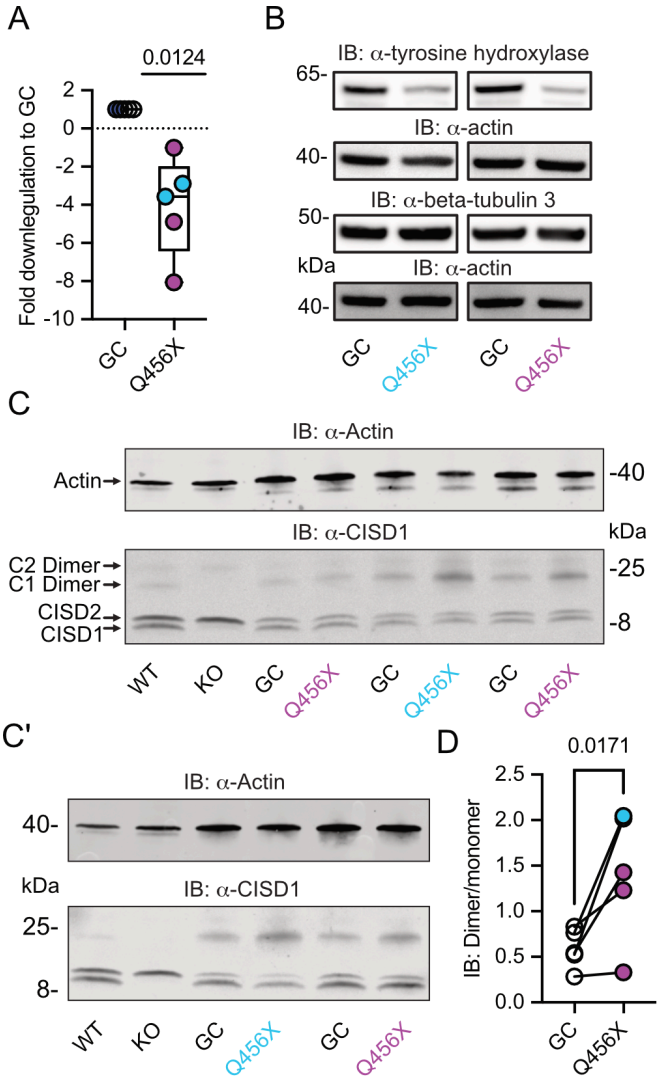

Figure 1 Increased CISD1 dimer formation in human dopaminergic neurons from PD patients with a *PINK1* Q456X mutation.

A. Quantitative PCR analysis of *PINK1* mRNA expression in iPSC-derived dopaminergic neurons from PD patients carrying the *PINK1* Q456X mutation, colors indicate two different patients. *ACTB* served as housekeeping control. Expression levels were normalized to gene-corrected (GC) controls.

B. Immunoblots of tyrosine hydroxylase as a marker for dopaminergic neurons and beta-tubulin 3 as a general neuronal marker. Actin served as loading control, size is indicated.

C and C'. Immunoblots of CISD1 and CISD2 with lysates from different patients, GC controls, and independent differentiations over 28 days *in vitro*. Monomeric and dimeric forms of both proteins are indicated by arrows. CISD1 knockout (KO) and wildtype (WT) mouse embryonic fibroblasts served to identify the correct bands. Actin served as loading control, size is indicated.

D. Quantification of the dimer/monomer ratio reveals an increased ratio in *PINK1* Q456X dopaminergic neurons over gene-corrected controls. Each data point corresponds to an independent differentiation over 28 days and the colors designate the two different patients.

Data in A were normalized to the respective gene-corrected control and are presented as box and whisker plots with the box extending from the 25th to the 75th percentile and the whiskers from the minimum to the maximum value depicting all individual data points. Data points in D correspond to the mean of two independent technical replicates of the five independent differentiations from two patients and are unnormalized. Statistical analysis was done using the one-sided t test in A and a nested t test in D, *p* values are indicated.

Our immunoblots revealed no changes in the abundance of CISD1 or CISD2. However, we clearly observed an increased presence of the CISD1 dimer in mutant *PINK1* neurons. Notably, both patients exhibited an elevated dimer/monomer ratio with variations in each individual differentiation in patient #1, and a more pronounced effect in patient #2, implying the presence of additional patient-specific factors. When pooled together, this analysis revealed a significant increase in CISD1 dimerization in mutant *PINK1* neurons compared to gene-corrected controls (Figure 1D). This heightened propensity for dimer formation therefore appears to be relevant for human Parkinson's disease.

CISD1 lacking its iron-sulfur cluster has a higher propensity to dimerize

To next clarify under which conditions CISD1 exhibits a heightened propensity to run as a dimer, we developed a split luciferase assay to investigate CISD1 dimerization in living cells in a dynamic and reversible manner (Dixon *et al*, 2016). We fused CISD1 with the two small subunits of NanoLuc luciferase, enabling us to quantify dimerization by measuring luminescence. Given the labile nature of CISD1's iron-sulfur cluster due to its unconventional coordination by one histidine and three cysteines, we hypothesized that the presence or absence of this cluster might influence dimerization. We therefore mutated histidine 87 to cysteine (H87C) which results in a more stable 2Fe/2S complex coordination. Conversely, the mutation of cysteine 83 to serine (C83S) completely abolishes the ability of CISD1 to bind the 2Fe/2S complex. By comparing the dimerization patterns of the CISD1 variants, we observed a significant increase in dimerization for C83S CISD1, the mutant incapable of binding the iron-sulfur cluster (Figure 2A). This finding suggested that iron-depleted CISD1 has a higher propensity for dimerization. To further validate these findings, we next employed an *in silico* approach to calculate the molecular hydrophobicity potential and the angle of rotation between two CISD1 models or two CISD1 C83S models (Polyansky *et al*, 2014). This analysis unveiled a larger surface-surface contact between the C83S monomers, indicating a closer binding compared to wildtype CISD1 (Figure 2B). This aligns with the results from the dimerization assay (Figure 2A).

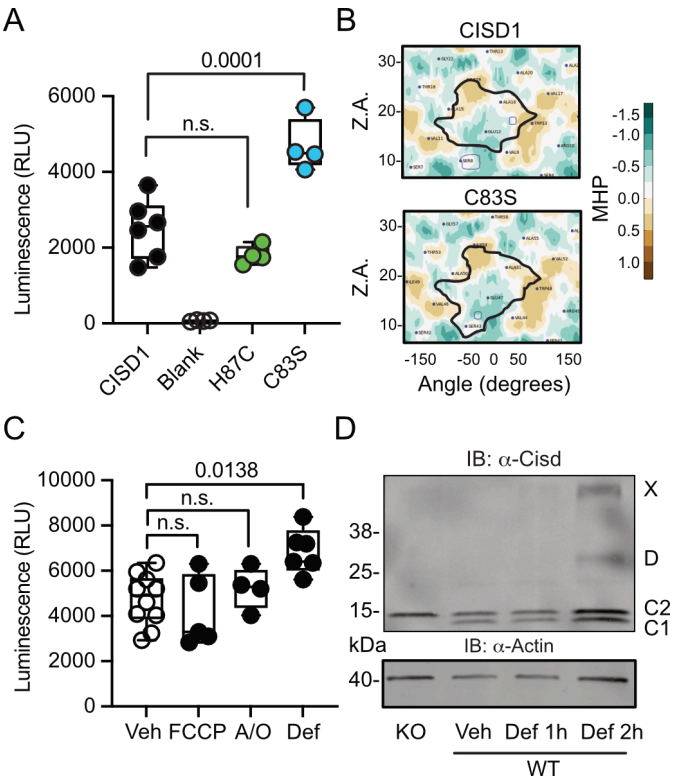

Figure 2 CISD1 lacking its iron-sulfur cluster has a higher propensity to dimerize.

A. Cells were transiently transfected with wildtype or point-mutated CISD1 tagged with split NanoLuc fragments and luminescence quantified 48 h later.

B. 2D maps of the molecular hydrophobicity potential (MHP) on the peptide surfaces in two CISD1 models or two C83S models. Dimerization interfaces are outlined. Axis values correspond to the rotation angle around the helical axis (α) and the distance along the latter (Z), 2D maps are colored according to MHP arbitrary units. The surface-surface area is indicated by a solid line.

C. Cells were transiently transfected with wildtype CISD1 tagged with split NanoLuc fragments and treated for 2 h with 1 μM FCCP, 2.5 μM antimycin and oligomycin (A/O), or 1 mM deferiprone (Def) before addition of substrate and quantification of luminescence.

D. Immunoblot of wildtype (WT) MEF cells treated for the indicated period of time with 1 mM Def or vehicle (Veh). Knockout (KO) cells served as control for antibody specificity and actin as loading control.

Each data point in A and C are from 5 independent experiments done in triplicates. Data are presented as box and whisker plots with the box extending from the 25th to the 75th percentile and the whiskers from the minimum to the maximum value depicting all individual data points. Statistical analysis was done using one-way ANOVA, *p* values are indicated.

Based on these findings, we hypothesized that conditions that induce mitophagy might yield a similar increase in dimerization. To investigate this, we conducted our dimerization assay in cells subjected to a two-hour treatment with the uncoupling agent carbonyl cyanide-p-trifluoromethoxyphenylhydrazone (FCCP), a combination of the complex V inhibitor oligomycin and the complex III inhibitor antimycin A (A/O), or the iron chelator deferiprone (Def), which triggers a distinct form of mitophagy independent of PINK1 and PRKN (Allen *et al*, 2013). The two-hour treatment was chosen to exclude alterations caused by degradation of CISD1. Remarkably, our results demonstrated that under these conditions only iron chelation resulted in increased dimerization (Figure 2C) that mirrored the increased dimerization seen in the C83S mutant, which is unable to bind the 2Fe/2S complex (Figure 2A). To corroborate this, we expanded our analysis to wildtype MEF cells treated with deferiprone. Immunoblotting revealed increased dimer formation and even the presence of a CISD1 multimer under these conditions (Figure 2D). Consequently, we conclude that the increased dimer formation in the *PINK1* mutant neurons likely represents the presence of apo-CISD1, a form of CISD1 devoid of its iron-sulfur cluster, and that this is caused by changes in the iron homeostasis.

Iron-depleted apo-CISD1 is not capable of rescuing increased mitochondrial fragmentation and oxidative distress in *Cisd1* KO mouse cells

To clarify whether apo-CISD1 plays a role in mediating part of the detrimental phenotype observed in PINK1 pathology, we investigated its effect on two previously reported phenotypes associated with *Cisd1* KO: increased mitochondrial fragmentation (Vernay *et al*, 2017) and heightened oxidative distress (Geldenhuys *et al*, 2017). KO cells indeed exhibited a decrease in tubular mitochondria, quantified by high-content imaging of cells stained with Mitotracker Green (Figure 3A), and elevated levels of cellular reactive oxygen species, as determined by the CellRox sensor stain (Figure 3B). CellRox detects superoxide (O_2^-) and hydroxyl radicals (•OH) similar to the dihydroethidium stain used by Geldenhuys et al. (Geldenhuys *et al*, 2017). We stably reconstituted KO cells with empty vector (EV) or HA-tagged wildtype or C83S CISD1 to investigate how apo-CISD1 influences these phenotypes. Consistent with our earlier observations, C83S CISD1 mainly occurred as a dimer, while wildtype CISD1 exhibited both monomeric and dimeric forms (Figure 3C). Note that untransfected cells displayed only faint CISD1 dimer bands suggesting that the absolute amounts of CISD1 affects its propensity to form dimers. When we assessed mitochondrial shape and ROS levels, we observed significant differences between cells rescued with wildtype CISD1 and those expressing CISD1 C83S. Cells reconstituted with wildtype CISD1 displayed a greater abundance of tubular mitochondria and lower levels of reactive oxygen species compared to C83S-expressing cells (Figure 3D/E). However, even wildtype CISD1 was unable to fully restore the phenotype to that of wildtype cells, suggesting the presence of additional alterations in the KO cells that are independent of CISD1. Furthermore, due to the already pronounced mitochondrial fragmentation and elevated ROS levels in KO cells, it was challenging to discern any additional detrimental effects of CISD1 C83S, possibly due to a ceiling effect. In summary, these data strongly imply that the iron-sulfur cluster of CISD1 is indispensable for CISD1's role in regulating mitochondrial morphology and defending against oxidative stress.

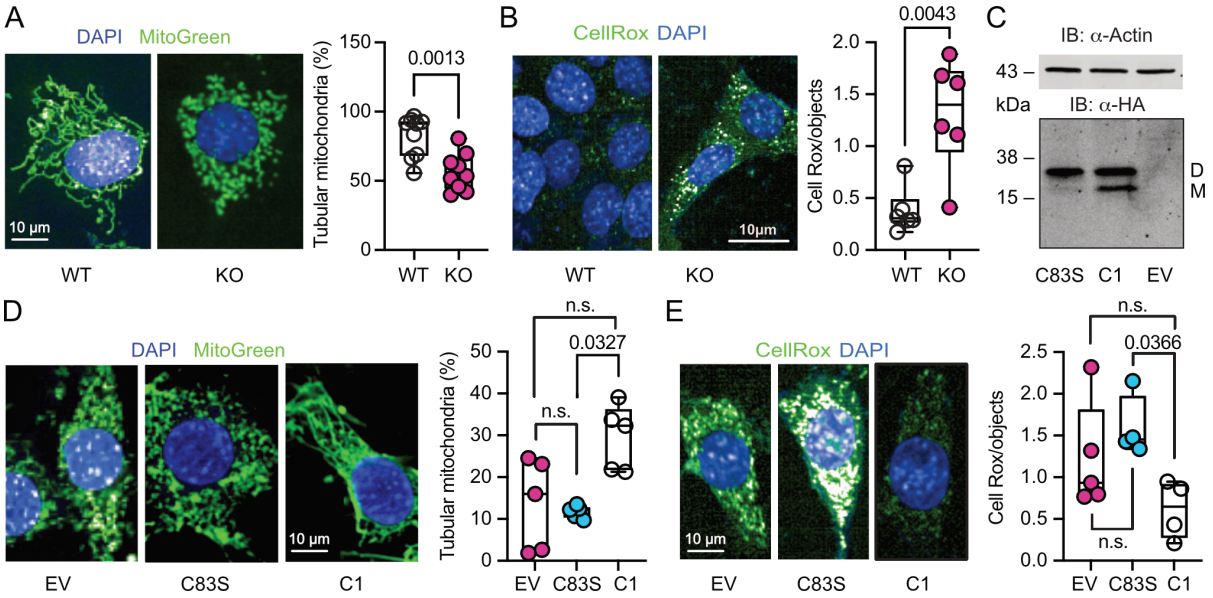

Figure 3 Iron-depleted apo-CISD1 is not capable of rescuing increased mitochondrial fragmentation and oxidative distress in CISD1 KO mouse cells.

A/D. Representative images of automated high-content confocal microscopy of Mitotracker Green stained MEF cells and results of automated quantification of tubular mitochondria normalized to the number of nuclei.

B/E. Representative images of automated high-content confocal microscopy analysis of oxidative stress in the cytosol measured by the dye CellRox™ and automated quantification.

C. Immunoblot of CISD1 KO cells stably transfected with HA-tagged wildtype (C1) and C83S CISD1. Empty vector (EV) served as negative control and Actin as loading control, size is indicated. (M) monomer and (D) dimer of CISD1.

Data in A are from 9 independent experiments done in triplicates from wells containing a range of 300 to 2000 cells each. Data in B-D are from 5 independent experiments done in triplicates from wells containing a range of 300 to 2000 cells each. Data are presented as box and whisker plots with the box extending from the 25th to the 75th percentile and the whiskers from the minimum to the maximum value depicting all individual data points. Statistical analysis was done using the student's *t* test in A/B and one-way ANOVA in D/E, *p* values are indicated.

Overexpression of Cisd and apo-Cisd in *Drosophila* is detrimental

To investigate the potential detrimental effects of C83S expression in vivo, we conducted experiments using *Drosophila melanogaster*, a model that has been instrumental in elucidating the function of PINK1 and PRKN. We generated flies that ubiquitously overexpressed either *wildtype* or *C111S Cisd* (the residue corresponding to human C83) and first examined development and lifespan. The *da* (*daughterless*)-Gal4 driver line served to induce ubiquitous, mild overexpression while strong ubiquitous overexpression was achieved by the *tubP* (*tubulin*) promoter. Already mild ubiquitous overexpression resulted in a significant reduction in lifespan compared to control flies aligning with prior findings (Chen *et al*, 2020). However, overexpressing *wildtype Cisd* or *C111S Cisd* had the same effect (Figure 4A). We therefore restricted our investigation of the impact of strong ubiquitous overexpression driven by the tubulin promoter on the developmental period. Here we observed a clear difference between *wildtype* and *C111S Cisd*; overexpressing *C111S Cisd* significantly prolonged the developmental period until eclosion to adult flies while *wildtype Cisd* or various controls had no discernible effect (Figure 4B). These findings align with previous data suggesting that prolonged development in flies is associated with oxidative distress (Lozinsky *et al*, 2013).

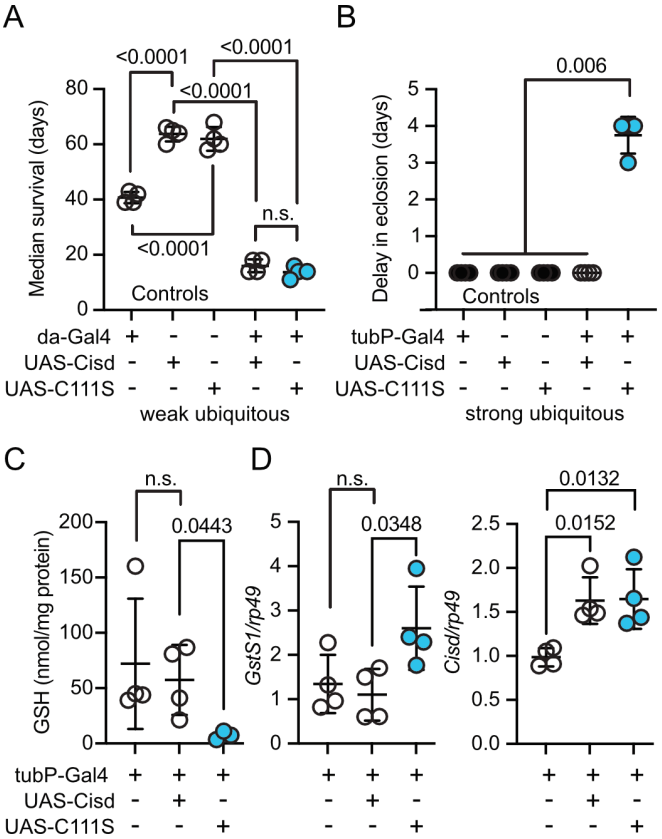

Figure 4 Overexpression of *Cisd* and *apo-Cisd* in Drosophila is detrimental.

A. Median survival of flies overexpressing *Cisd* or *C111S Cisd* (corresponding to human C83S) on standard food. Overexpression was achieved using the UAS>>Gal4 system and the mild ubiquitous *daughterless (Da)* driver line. Fresh food was supplied and the number of dead flies was scored every two days. Each dot represents the median lifespan of a group of 25 flies.

B. Delayed development until eclosion of adult flies overexpressing *C111S Cisd* using the UAS>>Gal4 system and the strong tubulin (tubP) driver line. Controls are indicated.

C. Enzymatic quantification of total glutathione (GSH and GSSG) levels normalized to protein in newly eclosed flies. 5 flies were used per sample.

D. Quantitative PCR analysis of *GstS1* and *Cisd* mRNA levels in newly eclosed flies. Rp49 served as housekeeping control. Each dot represents the mean relative transcriptional level of a sample of five flies. The values were normalized to the mean value of control flies (*TubP-Gal4*).

Statistical analysis was done using one-way ANOVA in A-C and the student's *t* test in D/E, *p* values are indicated.

In line with that, newly eclosed flies expressing *C111S Cisd* displayed significantly lower total glutathione (comprising both reduced GSH and oxidized GSSG) levels (Figure 4C). These flies also showed upregulated mRNA levels of the glutathione S-transferase S1 (*GstS1*) gene while expression levels of *Cisd* and *C111S Cisd* were similar (Figure 4D) but much lower than expected considering the strong induction by the *tubP* promoter. This might constitute a compensatory adaptation to the detrimental effect of forced overexpression of *Cisd*. This is also in line with the fact that only very few flies eclosed under these conditions which we considered as escapees. The upregulation of *GstS1* is probably part of an activated antioxidant response as *GstS1* was identified previously in an unbiased genetic screen for genes that modify parkin phenotypes. It was also shown that overexpression of *GstS1* in dopaminergic neurons suppresses neurodegeneration in parkin mutants (Whitworth *et al*, 2005; Greene *et al*, 2005). In summary, our findings collectively suggest a potentially adverse impact of both wildtype and iron-depleted Cisd. Under conditions of robust expression, apo-Cisd appears to exert a more pronounced deleterious effect. It is noteworthy that the levels of apo-Cisd seem to play a pivotal role in influencing redox homeostasis, as discerned from the observed alterations in glutathione levels.

Increased Cisd dimer levels and altered iron homeostasis in *Pink1* mutant flies

We next investigated whether *Pink1* loss of function in flies mirrors the human situation and impacts Cisd dimerization or possibly abundance. $Pink1^{B9}$ flies (Park *et al*, 2006) are on the w^{1118} background and have a large deletion of the coding region and almost no remaining mRNA expression (supplemental Figure 1). At the mRNA level, we observed no changes in *Cisd* mRNA levels in $Pink1^{B9}$ flies (Figure 5A). We then immunoblotted samples from young (3 day-old) and old (8 week-old) wildtype w^{1118} and $Pink1^{B9}$ flies and noted that fly Cisd, similar to mouse CISD1, runs as a monomer and dimer even on reducing gels containing dithiothreitol (DTT) (Figure 5B). Extremely reducing conditions of prolonged incubation with higher concentrations of DTT and tris-(2-carboxyethyl)-phosphine as a disulfide-bond breaking agent followed by boiling, however, resulted in loss of dimeric and an increase of monomeric Cisd (supplemental Figure 2) indicating that the dimer is indeed most probably a dimer and does not represent a posttranslational modification or an artifact. We quantified total Cisd protein levels i.e. monomer plus dimer and normalized them to actin. Additionally, we assessed the dimer/monomer ratio. This analysis unveiled reduced total Cisd protein levels in young *Pink1* mutant flies compared to *wildtype* flies (Figure 5C). We were unable to replicate the previously reported age-dependent increase in Cisd abundance in wildtype flies (Chen *et al*, 2020) although this was evident in many but not all samples indicating additional factors. When assessing the dimer/monomer ratio, we observed a significant increase in dimer levels in old $Pink1^{B9}$ flies compared to young $Pink1^{B9}$ flies and old wildtype flies (Figure 5D). Age had no effect on dimerization of wildtype flies (Figure 5D). Thus, *Pink1* mutant flies manifest analogous alterations to those observed in dopaminergic neurons from patients afflicted by familial Parkinson's disease due to PINK1 Q456X mutation (Figure 1D).

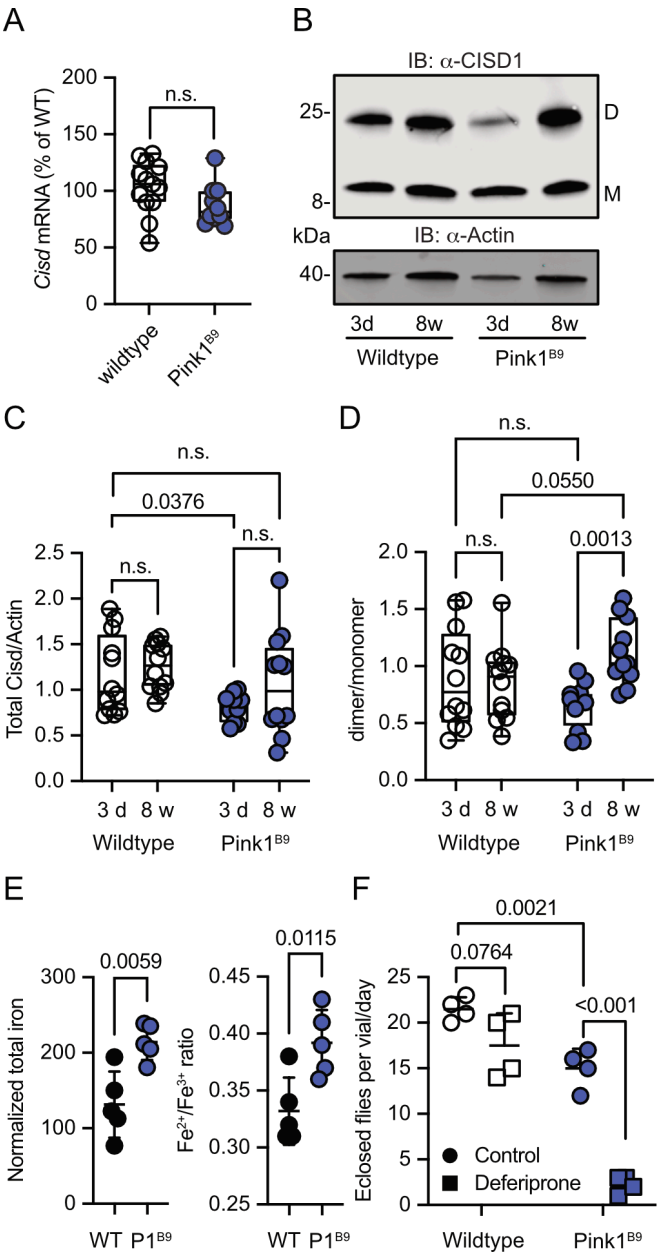

Figure 5 Increased Cisd dimer levels and altered iron homeostasis in *Pink1* mutant flies.

A. Quantitative PCR analysis of *Cisd* mRNA levels in *Pink1*^{B9} flies. *RpL32/Rp49* served as housekeeping control. Each dot represents the mean relative transcriptional level of a sample of five flies. The values were normalized to the mean value of wildtype flies.

B. Immunoblot analysis of Cisd abundance in the indicated fly strains at different ages, 3 days (d) and 8 weeks (w). Actin served as loading control, size is indicated. (M) Cisd monomers and (D) dimers.

C. Total Cisd (D+M) normalized to actin. Each dot represents the mean of two technical replicates from n=12 independent samples of two male flies.

D. Dimer/monomer ratio of the same samples.

E. Total iron content and Fe^{2+}/Fe^{3+} ratio measured via CE-ICP-MS in WT and Pink1^{B9} flies. Each dot represents a group of 3 male flies. n=5.

F. Flies of the same age, number and sex ratio were allowed to mate and lay eggs in normal food or food prepared with a 65 µM final concentration of deferiprone. Each dot represents the average number of eclosed flies per vial and day for three consecutive days.

Data are presented in A/C/D as box and whisker plots with the box extending from the 25th to the 75th percentile and the whiskers from the minimum to the maximum value depicting all individual data points and as scatter plots with the mean and SD in E/F. Statistical analysis was done using one-way ANOVA in A, two-way ANOVA in C/D and student's *t* test in E/F, *p* values are indicated.

Having demonstrated that iron dyshomeostasis induced by the iron-depleting agent deferiprone results in increased CISD1 dimer formation in fibroblasts, we next investigated iron dynamics in *Pink1* mutant flies compared to controls by employing mass spectrometry. This revealed a heightened total iron content in Pink1 mutants (Figure 5E). Delving deeper with capillary electrophoresis-inductively coupled plasma mass spectrometry (CE-ICP-MS), we then identified an enrichment of redox-active Fe^{2+} ions in these mutants compared to the more subdued presence of redox-inactive Fe^{3+} (Figure 5E). In the Fenton reaction, ferrous iron (Fe^{2+}) forms hydroxyl radicals (•OH), a highly reactive and destructive free radical, and ferric iron (Fe^{3+}) in the presence of hydrogen peroxide. *Pink1*^{B9} flies are therefore in a more pro-oxidative state. *Pink1*^{B9} flies were also dramatically more susceptible to iron depletion with deferiprone. In these experiments, we fed developing *wildtype* and Pink1 mutant flies food supplemented with 65 µM deferiprone, a concentration that did not induce widespread mitophagy in *Pink1* flies (Lee *et al*, 2018), and quantified the number of adult flies eclosing from pupae. This revealed that iron depletion also showed a trend towards reduced eclosion of wildtype flies but nearly completely abrogated the eclosion of *Pink1* mutant flies (Figure 5F). Collectively, these results support a connection between iron dyshomeostasis, redox imbalance, and the presence of apo-Cisd, although establishing causality in this relationship is challenging.

Cisd depletion rescues *Pink1* mutant phenotypes

To clarify whether depleting the potentially detrimental (apo) Cisd could mitigate Pink1 pathology, we first used a ubiquitous knockdown of *Cisd* in *Pink1*^{B9} mutant flies by RNAi driven by the tubulin driver focusing on lifespan as a readout. Because *Pink1* resides on the fly heterosome, hemizygous male flies represent a complete KO while heterozygous female flies still retain one functional allele and serve as controls. Knockdown of *Cisd* led to an approximately 60% reduction of Cisd protein levels (supplemental figure 3A/B). Importantly, this knockdown effectively rescued the reduced lifespan (supplemental figure 3C) of *Pink1* mutant males, suggesting a detrimental effect of *Cisd* in flies lacking *Pink1*. To rule out any potential unspecific effects resulting from RNAi, we subsequently generated a complete knockout of the entire genomic sequence of *Cisd* in w^{1118} flies using CRISPR/Cas9 technology (supplemental figure 4A). Flies devoid of Cisd protein expression exhibited no discernible difference in climbing ability up to 30 days of age (supplemental figure 4B) and only a minor reduction in lifespan (supplemental figure 4C). This contrasts with a previously reported Cisd null mutant generated by transposon integration (*Cisd2*^{G6528}), which was shown to increase lifespan (Chen *et al*, 2020). The complete knockout allowed us to observe that Cisd runs as a monomer (M), a dimer (D) as shown and quantified earlier, but also as a weak multimer (X) (Figure 6a) akin to what we observed in deferiprone-treated fibroblasts (Figure 2D). Given the unavailability of functional antibodies against fly Pink1, we quantified *Pink1* mRNA levels to verify the loss of *Pink1* expression in *Pink1*^{B9} flies and to investigate potential dysregulations in *Cisd* KO flies. *Pink1* levels were reduced in *Pink1*^{B9} but unchanged in *Cisd* KO flies (Figure 6B). We then investigated the effect of complete Cisd depletion on the phenotypes described in mutant *Pink1*^{B9} flies including reduced dopamine levels, lifespan, climbing ability, a morphological wing phenotype caused by atrophy of the wing muscles, and an altered mitochondria ultrastructure (Clark *et al*, 2006; Park *et al*, 2006). As expected, *Pink1*^{B9} flies exhibited reduced climbing ability (Figure 6C), an abnormal wing posture (Figure 6D), a decreased lifespan (Figure 6E), and diminished dopamine levels (Figure 6F) in line with prior reports (Clark *et al*, 2006; Park *et al*, 2006). We then generated double-knockout flies (DKO) lacking both *Cisd* and *Pink1*, with the loss of Cisd expression shown in supplemental figure 5. Remarkably, when compared to *Pink1*^{B9} flies these DKO flies exhibited normal climbing ability, normal wing morphology, normal dopamine levels, and a normal lifespan, essentially representing a complete rescue of these phenotypes (Figure 6C-F).

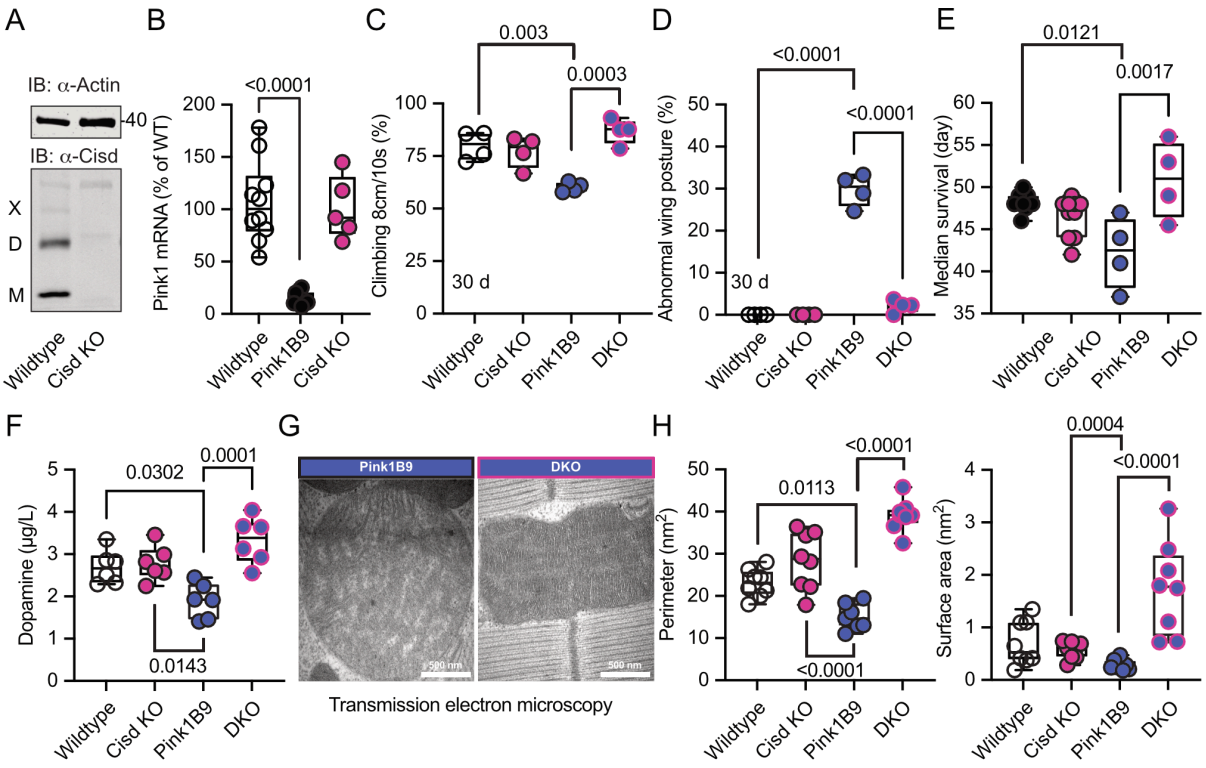

Figure 6 *Cisd* depletion rescues *Pink1* mutant phenotypes.

A. Immunoblot analysis of Cisd expression in wildtype and Cisd knockout (KO) flies, actin served as loading control. Note the presence of Cisd monomers (M), dimers (D), and multimers (X).

B. Quantitative PCR (qPCR) analysis of *Pink1* mRNA levels. *RpL32/Rp49* served as housekeeping control. Each dot represents the mean relative transcriptional level of a sample of five flies. The values were normalized to the mean value of wildtype flies.

C. Climbing ability. DKO, double knockout flies. Each dot represents the percentage of a group of 25 flies that climbed more than 8 cm within 10 s.

D. Abnormal wing posture evaluation. Percentage of flies with an abnormal wing posture. Each dot represents an individual trial of a group of 25 flies.

E. Median survival on standard food. Fresh food was supplied and the number of dead flies was scored every two days. Each dot represents the median lifespan of a group of 25 flies.

F. Dopamine levels quantified by HPLC. Each dot represents a group of 4 flies sampled at different days.

G. Representative transmission electron microscopy of flight muscle morphology from Pink1 mutant and DKO flies. Scale bar as indicated. Exemplary pictures from wildtype and *Cisd* KO flies are shown in supplemental figure 4.

H. Quantification of the indicated parameters. Each dot represents the average values from one image from 2 flies per genotype that were used for the analysis.

Data are presented as box and whisker plots with the box extending from the 25th to the 75th percentile and the whiskers from the minimum to the maximum value depicting all individual data points. Statistical analysis was done using one-way ANOVA, *p* values are indicated.

We further investigated whether these favorable effects of *Cisd* KO directly influenced mitochondria or stemmed from alternative non-mitochondrial factors. Flight muscles are densely populated with mitochondria and have been previously shown to be significantly impacted by the *Pink1*^{B9} mutation (Clark *et al*, 2006; Park *et al*, 2006). In *Pink1*^{B9} flies, flight muscles are atrophied and mitochondria cover less space, are smaller, and have a significantly reduced number of cristae resulting in a reduction of cristae surface (Figure 6G, a comparison of all four genotypes is shown in supplemental Figure 6). Intriguingly, the concurrent *Cisd* KO effectively rescued all these phenotypes (Figure 6H). Together these data strongly suggest that Cisd, most probably apo-Cisd, assumes a toxic function in *Pink1* mutant flies and serves as a critical mediator of Pink1-linked phenotypes, including the disruption of the normal mitochondria and cristae morphology.

Cisd gene reduction partially protects *Prkn* knockout flies

Pink1^{B9} and *Prkn* mutant flies (named *Park*^{25}, also w^{1118} background (Park *et al*, 2006)) exhibit remarkably similar phenotypes, and previous elegant work in flies established that *Pink1* functions upstream of *Prkn* (Clark *et al*, 2006; Park *et al*, 2006). Furthermore, Cisd is the most prominent *Prkn* target in flies (Martinez *et al*, 2017). We therefore next investigated whether *Prkn* mutation also affects Cisd abundance or dimerization and whether loss of *Cisd* also protects against *Prkn* loss-of-function pathology. Given the absence of functional antibodies against fly Prkn, we used quantitative PCR to verify *Prkn* depletion in *Prkn* mutant flies. As expected, *Park*^{25} flies expressed no *Prkn* mRNA, but, intriguingly, *Cisd* mRNA was also dramatically reduced in Prkn mutant flies (Figure 7A). Similarly, *Prkn* mRNA was nearly undetectable in *Cisd* knockout flies (Figure 7B). When we examined total Cisd protein levels, we observed a downregulation of total Cisd levels in both young and old *Prkn* mutant flies in line with the mRNA results (Figure 7C). An exemplary blot is provided in figure 7C', a blot demonstrating Cisd depletion also in Prkn/Cisd DKO flies is shown in supplemental figure 3. The dimer/monomer ratio was unchanged and displayed again a considerable degree of variability (Figure 7D/D'). We concluded that the substantial regulation of *Prkn* mRNA in *Cisd* KO flies and *Cisd* mRNA and protein in *Park*^{25} flies suggests that these genes function within related pathways.

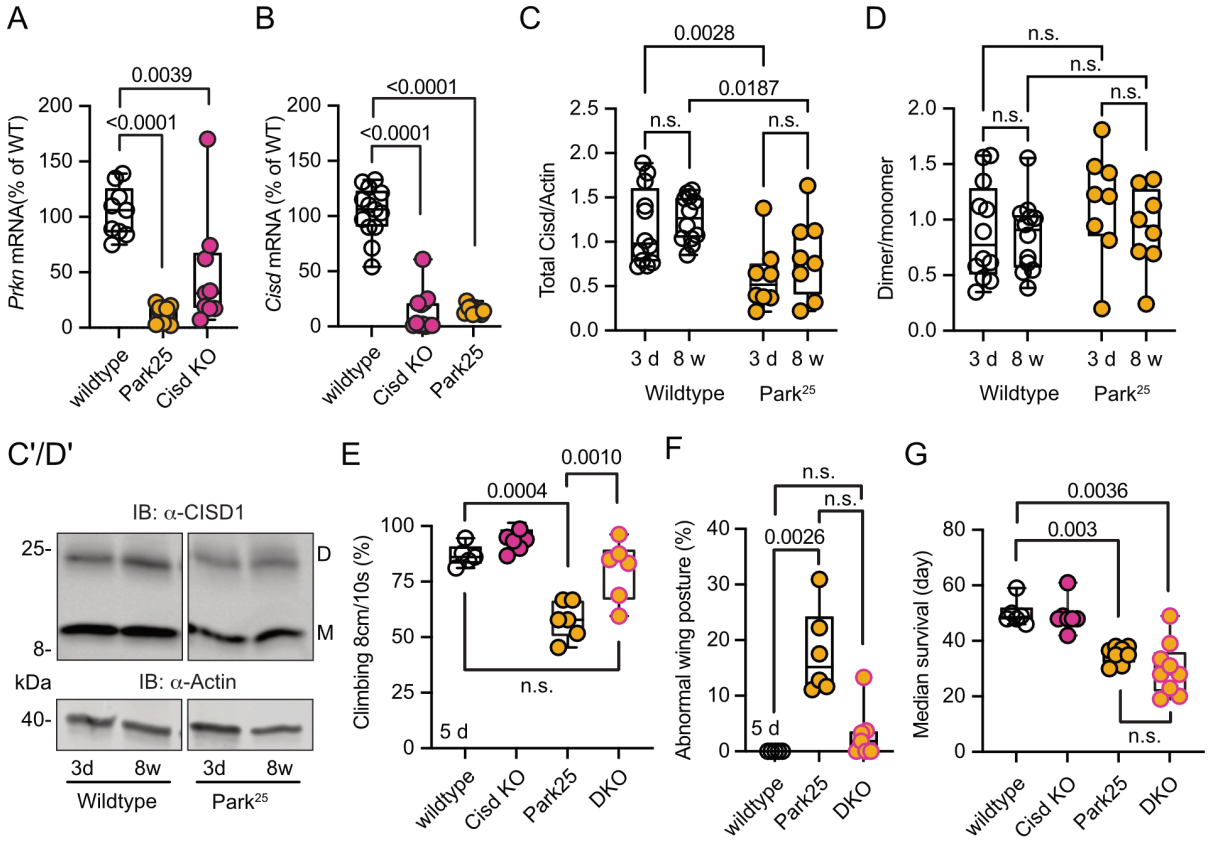

Figure 7 *Cisd* gene reduction partially protects *Prkn* knockout flies .

A/B. Quantitative PCR analysis of *Prkn* and *Cisd* mRNA levels in *Cisd* KO and Park^{25} flies. *RpL32/Rp49* served as housekeeping control. Each dot represents the relative transcriptional level of a sample of five flies. The values were normalized to the mean value of wildtype flies.

C. Total Cisd (D+M) normalized to actin. Each dot represents the mean of two technical replicates from n=12 wildtype and n=8 Park^{25} independent samples of two male flies. The wildtype samples shown for comparison are the same as in Figure 5c/d.

D. Dimer/monomer ratio of the same samples.

C'/D'. Immunoblot analysis of Cisd abundance in the indicated fly strains at different ages, 3 days (d) and 8 weeks (w). Actin served as loading control, size is indicated. (M) Cisd monomers and (D) dimers. The gap indicates the removal of the Pink1^{B9} samples shown in Figure 5 that were run on the same blot.

E. Climbing ability assessment. Each dot represents the percentage of a group of 25 flies that successfully climbed more than 8 cm within 10 s.

F. Abnormal wing posture evaluation. Percentage of flies with an abnormal wing posture. Each dot represents an individual trial of a group of 25 flies.

G. Median survival on standard food. Fresh food was supplied and the number of dead flies was scored every two days. Each dot represents the median lifespan of a group of 25 flies.

Data are presented as box and whisker plots with the box extending from the 25th to the 75th percentile and the whiskers from the minimum to the maximum value depicting all individual data points. Statistical analysis was done using one-way ANOVA in A/B/F/G and two-way ANOVA in C/D, *p* values are indicated.

Similarly to *Pink1*^{B9} flies, *Park*^{25} flies exhibited a notable reduction in climbing ability (Figure 7E), an abnormal wing posture (Figure 7F), and a shortened lifespan (Figure 7G), consistent with previous reports (Clark *et al*, 2006; Park *et al*, 2006). Intriguingly, concurrent Cisd KO conferred complete protection against the climbing impairment of *Park*^{25} flies (Figure 7E) and showed a distinct inclination towards normal wing posture with DKO being not significantly different from wildtype flies (Figure 7F). However, surprisingly, DKO did not rescue the lifespan of *Park*^{25} flies (Figure 7G). This observation suggests that Cisd likely serves an essential, yet undiscovered, function, particularly in the aging fly, and its loss is compensated for in the presence of Prkn.

Discussion

We here identified the mitochondrial protein CISD1, specifically its iron-depleted form, as a potential downstream mediator of the pathophysiological effects arising from the loss of PINK1 function, and to a certain extent, Parkin loss of function.

Our investigation revealed that both dopaminergic neurons from familial Parkinson's disease patients with *PINK1* mutations and *Pink1* mutant flies exhibit increased levels of a slower-migrating form of CISD1/Cisd on immunoblots. Ths increase was age-dependent in the flies and apparent in human dopaminergic neurons after 28 days of differentiation. We did not assess whether dimerization would be even stronger in older cultures but such an age-dependent increase would be in line with the fact that PD usually becomes symptomatic at an older age. We consider this slower-migrating form of CISD1/Cisd to be a CISD1 with a higher propensity to dimerize because it has lost its iron-sulfur cluster. The iron-sulfur cluster of CISD1 is easily lost because it is coordinated in an unconventional manner by one histidine (H) and three cysteines (C) instead of the more common 2H/2C or 4C coordination (Wiley *et al*, 2007b). This serves to transfer the iron-sulfur cluster to other proteins as part of a cellular adaptive response that helps recovery from oxidative injury (reviewed in (Mittler *et al*, 2019)). We confirmed that iron-depleted CISD1, apo-CISD1, has a higher propensity to dimerize by genetically engineering CISD1 to be incapable of binding the iron-sulfur cluster and by treating cells with the iron-depleting agent deferiprone, both of which increased dimer formation compared to controls. This was demonstrated using a cellular assay based on complementation of split luciferase and immunoblots. Importantly, the slower-migrating form likely does not represent a ubiquitinated form, as treatment with the deubiquitinase USP2 had no effect on Cisd dimerization (Martinez *et al*, 2023). Additionally, it is improbable that the slower-migrating Cisd form is an unrelated protein, as under non-reducing conditions, fly Cisd shifted to the dimeric form (Martinez *et al*, 2023) while harsh reducing conditions shifted Cisd to the monomeric form (supplemental Figure 2). Interestingly, other agents that trigger mitophagy had no effect on CISD1 dimerization in our experimental setting. We can certainly not rule out that additional factors, e.g. changes in other post-translational modifications like phosphorylation favor increased CISD1/Cisd dimerization.

Our results suggest that apo-CISD1 exhibits a potential toxic gain of function. Interestingly, prolonged exposure of mouse embryonic fibroblasts to the iron depleting agent

2,2′-bipyridine results in downregulation of Cisd1 (Key *et al*, 2020) possibly as a compensatory mechanism to limit the abundance of such a toxic iron-depleted CISD1. In mouse cells, the overexpression of a genetically engineered apo-CISD1 mutant, but not of wildtype CISD1, in knockout cells leads to heightened mitochondrial fragmentation and elevated cellular reactive oxygen species levels. However, these negative effects closely resembled the changes observed in knockout cells, posing challenges in discerning additional detrimental effects due to a potential ceiling effect. In line with this assumption, overexpressing mutant *apo-Cisd* but not wildtype *Cisd* in flies disrupts redox homeostasis and negatively impacts development. However, both Cisd species significantly shortened lifespan when overexpressed in wildtype adult flies implying that even wildtype *Cisd* can acquire a toxic function. Removing fly Cisd by knockout of the coding sequence completely protected flies against Pink1 depletion-induced changes in climbing ability, abnormal wing posture, dopamine levels and lifespan but ameliorated only the climbing ability and wing posture in Parkin mutant flies. Previous work demonstrated that ectopic overexpression of Cisd in muscle, decreased the lifespan of flies and resulted in enlarged mitochondria containing numerous intramitochondrial vesicles surrounded by a double membrane (Chen *et al*, 2020). Our data now indicate that this process might contribute to the pathophysiology resulting from the loss of Pink1/Prkn-mediated mitochondrial quality control. Very recent work, published during the revision of this manuscript, discovered that both genetic and pharmacologic suppression of CISD1 and Cisd restored increased ER calcium release conferred by *PINK1* and *Parkin* mutation in mammalian cells and flies (Ham *et al*, 2023). However, the specific role of apo-Cisd in this remains to be fully elucidated.

Our data possibly implicate the accumulation of iron-depleted CISD1, referred to as apo-CISD1, in the pathogenesis of human disease. We propose that the toxicity of apo-CISD1 involves changes in iron homeostasis and redox dyshomeostasis, hallmarks of Parkinson's disease. Holo-CISD1 is capable of transferring its 2Fe/2S cluster to other proteins like IRP1, as previously demonstrated (Ferecatu *et al*, 2014). Also in flies, Cisd physically interacts with holo-IRP1, and its deficiency renders flies more susceptible to iron depletion (Huynh *et al*, 2019), as also observed by us for *Pink1* mutant flies. How apo-CISD1 is then reconstituted is rather unclear. A recent report suggested that CISD1 can receive its Fe/S cluster from its homologue CISD3 (aka MiNT) in the mitochondrial matrix via the porin VDAC1 (Karmi *et al*, 2022). So it appears possible that either this transfer is inhibited/attenuated or that the apo-CISD1/Cisd observed in Pink1 mutant dopaminergic neurons and Pink1 mutant flies constitutes a permanently fixed apo-CISD1/Cisd that cannot be reconstituted. One plausible scenario for this fixation is the oxidation of one of the coordinating cysteines, disrupting the process. This disruption could result in a defective recycling of cytosolic apo-IRP1 into holo-IRP1, leading on the one hand to a deficiency in cytosolic aconitase activity. Knockdown of CISD1 in cells indeed significantly reduces the cytosolic aconitase activity (Tan *et al*, 2016). On the other hand, apo-IRP1 not only lacks aconitase activity but also binds to iron-responsive elements (IREs) in the mRNA of iron-responsive genes (Haile *et al*, 1992b, 1992a). Association with IREs in the 5' untranslated region of ferritin mRNA inhibits Ferritin translation resulting in less bound iron and an increase in free iron (Chen *et al*, 1997) while association with IREs in the 3' untranslated region of the mRNA encoding the iron importers transferrin receptor 1 and SLC11A2 stabilizes the mRNAs and facilitates their translation resulting in increased iron import (Galy *et al*, 2010). Together the transcriptional changes caused by the presence of apo-IRP1 result in iron overload which is an important factor in the pathology associated with PD (recently reviewed in (Ma *et al*, 2021)). Our study also revealed increased total iron levels in Pink1 mutant flies. Notably, knockout of PINK1 in flies (Esposito *et al*, 2013), in mice

(Gautier *et al*, 2008), and in human dopaminergic neurons (Bus *et al*, 2020) also results in a reduced aconitase activity in mitochondria. Mitochondrial aconitase contains an iron-responsive element in its 5' untranslated region (Kim *et al*, 1996), making its expression subject to repression by apo-IRP1. The inactivation of mitochondrial aconitase caused by Pink1 loss of function triggers increased superoxide production, oxidative stress, and mitochondrial swelling (Esposito *et al*, 2013). Others reproduced these findings and reported that overexpression of mitoferrin, a mitochondrial iron transporter, mitigates the reduced mitochondrial aconitase activity, abnormal wing posture, flight deficits and mitochondrial morphology defects associated with Pink1 loss of function by elevating mitochondrial bioavailable iron levels (Wan *et al*, 2020). Interestingly, knockout of IRP2, a protein highly homologous to IRP1 but lacking aconitase activity, results in iron accumulation and Parkinsonism in mice (LaVaute *et al*, 2001). An interaction of CISD1 with IRP2 has not been reported so far but appears likely. In summary, these results strongly implicate altered mitochondrial iron homeostasis and redox dysregulation in fly and human models of Parkinson's disease and link it to CISD1 dysfunction. The accumulation of apo-CISD1/Cisd and the subsequent inability to repair defective IRP1/2 would place CISD1 upstream of the changes in iron homeostasis observed in PD and models of PD (Ma *et al*, 2021).

In flies, Cisd appears to function downstream of Pink1 and Prkn, and given the conservation of this pathway, it is plausible to extend these findings to human context. However, the question arises as to whether gene reduction of CISD1 is feasible in mammals. In mice, complete KO of Cisd1 leads to a phenotype characterized by a shortened stride length and decreased rotarod performance, which was even described as being "Parkinsonian" (Geldenhuys *et al*, 2017). This phenotype was attributed to a mitochondrial dysfunction, resulting in increased production of mitochondrial reactive oxygen species, elevated iron accumulation in the striatum, and subsequent loss of striatal dopamine (Geldenhuys *et al*, 2017), consistent with our results obtained in KO MEFs. Notably, the authors did not report a deleterious phenotype for heterozygous mice (Geldenhuys *et al*, 2017). Additional research revealed age-dependent downregulation of CISD1 in the heart and kidney, with constitutive cardiac-specific deletion of CISD1 leading to cardiac dysfunction at 12 months and heart failure after 16 months, preceded by altered mitochondrial morphology and increased mitochondrial reactive oxygen species (Furihata *et al*, 2021). Importantly, this study also reported no discernible phenotype in heterozygous KO mice. These findings collectively suggest that complete loss of function of mammalian CISD1 has deleterious effects, while partial inhibition or gene reduction, such as interfering with dimer formation, may hold therapeutic promise. Docking studies employing the reported crystal structure (Hou *et al*, 2007; Lin *et al*, 2007) were used to design and synthesize an inhibitor of CISD1 named NL-1 (Geldenhuys *et al*, 2010). NL-1 has shown promise in mouse models of traumatic brain injury (Yonutas *et al*, 2020), ischemic stroke (Saralkar *et al*, 2021), and lipopolysaccharide-induced inflammation (Lee *et al*, 2022b). It was even shown to induce mitophagy by promoting accumulation of PINK1 and Parkin (Lee *et al*, 2022a). Future studies will further explore the potential of NL-1 to mitigate the progression of Parkinson's disease in animal models and potentially in patients.

Our results suggest that the mitochondrial iron-sulfur cluster protein Cisd is downstream of the pathophysiological cascade initiated by Pink1 and partially Prkn loss of function in flies and probably also in humans. This sheds light on the pathophysiology of Parkinson's disease and implicates CISD1 as a therapeutic target protein.

Methods

Human dopaminergic neurons

Induced pluripotent stem cells (iPSCs) from two PD patients carrying the p.Q456X mutation in PINK1 were obtained from the University of Lübeck. Written informed consent is available at the University of Lübeck. For both mutant lines, isogenic gene-corrected controls have been successfully generated and characterized previously (Jarazo *et al*, 2022). Both PINK1-mutant and isogenic iPSCs were first converted into neuroepithelial stem cells (NESCs), based on the protocol previously described (Reinhardt *et al*, 2013). NESCs were cultivated in N2B27 medium (DMEM-F12/Neurobasal 50:50, supplemented with 1:200 N2, 1:100 B27 without vitamin A, 1% L-glutamine and 1% penicillin/streptomycin), containing 3 µM CHIR-99021, 0.5 µM purmorphamine (PMA) and 150 µM ascorbic acid. For the generation of midbrain-specific neurons, NESC maintenance medium was replaced by N2B27 containing 1 µM PMA, 200 µM ascorbic acid, 10 ng/ml BDNF, 10 ng/ml GDNF, 1 ng/ml TGF-b3 and 500 µM dbcAMP. After six days, differentiating NESCs were shifted to the same medium but without PMA (replaced every two days) and kept until day 28.

Immunoblotting

Cells were lysed in RIPA buffer (25 mM Tris•HCl pH 7.6, 150 mM NaCl, 1% NP-40, 1% sodium deoxycholate, 0.1% SDS) containing protease and phosphatase inhibitors. Cells were then centrifuged at maximum speed for 30 min at 4°C and the supernatant containing the whole-cell proteins was collected. Flies were isolated in the same buffer but were mechanically smashed with a dounce, centrifuged and the supernatant was collected. For reducing blots, protein samples were denatured in 1x Laemmli-sample-buffer (Tris-HCl, SDS, glycerol, bromophenol blue, and 50 mM DTT) whereas samples for non-reducing blots were denatured in 1x Laemmli-sample-buffer without DTT at 95 °C, 5 min. Harsh reducing conditions were generated by treating the samples with 100 mM DTT and 50 mM TCEP, incubation for 30 min at RT, and boiling for 10 min at 95°C. Proteins were separated by gel electrophoresis and transferred to nitrocellulose membranes using a semi-dry blotting system (Bio-Rad Laboratories). Membranes were blocked with 3% milk in TBST for 1 h at RT. Membranes were incubated with the respective antibodies overnight at 4°C, rotating. Antibodies used were rabbit anti-CISD1 (Proteintech, 1:1000), mouse anti-actin (Merck chemicals, 1:1000), rabbit anti-HA (Abcam, 1:1000), rabbit anti-TH (Millipore, AB152, 1:1000), mouse anti-TUBB3 (Biolegend, 801201, 1:20000), and mouse anti-β-actin (Cell signaling technology, 3700, 1:30,000). Fluorescence-labeled secondary antibodies were used at a 1:10,000 dilution, and the signal was detected using a Li-Cor Odyssey imaging system and quantified with the Image Studio Lite software. This imaging system is linear and oversaturation is indicated. The intensity was normalized to the loading control and the mean per blot.

Cell culture

MEF cell lines were grown in DMEM Glutamax (Gibco) supplemented with 10% (v/v) fetal calf serum (FCS; Thermo Scientific), 2 mM L-glutamine (Gibco), 1 x MEM non-essential amino acids, 100 U/ml penicillin and 100 µg/ml streptomycin (Gibco) in a humidified incubator at 37°C, 5% CO2 and 95% air. The MEF rescue and mutant cell lines were generated by Piggybac transposon-mediated genome integration followed by FAC sorting using a blue fluorescent protein (BFP2) expressed after a T2A site at the C-terminus of CISD1. C-terminal tags do not alter the function of CISD1 (Wiley *et al*, 2007a). Where indicated, cells were treated with deferiprone with a final concentration of 1 mM for 1 or 2 h.

Dimerization assay

Split nanoluc fragments LgBit and SmBit (Promega) were cloned N-terminally to human CISD1 and point mutations introduced by site-directed mutagenesis using the Q5 Site-Directed Mutagenesis kit (NEB). All plasmids were sequence verified. Experiments were carried out by transfecting HT22 cells with the plasmids for 48 hours after which 1 volume of the Nanoluc Live-Cell substrate was added with 19 volumes of Nano-Glo LCS Dilution Buffer. Where indicated, a final concentration of FCCP (1 µM), oligomycin/antimycin (2.5 µM each), deferiprone (1 mM (Allen *et al*, 2013)) or vehicle was added to the cells 2 h prior to the addition of the substrate.

Confocal microscopy and image analysis

High-content light microscopy was conducted with the Opera Phenix™ (Perkin Elmer) spinning disc microscope. Fluorescence (Ex/Em) for Hoechst 405/435-480 nm, MitoTracker™ Green FM 561/570-630 nm, and CellRox 485/520 nm was measured in a final concentration of 1 µM for 15 min, subsequently, cells were incubated with normal growth medium without phenol red dye. The images were analyzed with the software packages Harmony (version 4.5) and Columbus (version 2.7.1) containing the PhenoLOGICTM machine learning plugin (Perkin Elmer).The program was trained to recognize tubular or fragmented mitochondria. Individual cells were selected by nuclear staining with Hoechst and the cytosol was defined using the mitochondrial stain. Fluorescence intensity was measured and normalized to the number of cells counted per image.

Fly experiments

Cisd KO flies were generated by Wellgenetics (Taiwan, ROC) and contain the cassette depicted in supplemental Figure 2A. *Pink1*^{B9}, *Park*^{25}, *UAS-Cisd-WT*, *UAS-Cisd C83S* flies were a kind gift of Alex Whitworth (Mitochondrial Biology Unit, MRC, Cambridge, UK). *TubP-Gal4* (BDSC 5138), *Da-Gal4* (BDSC 8641), *Elav-Gal4* (BDSC 458), and *UAS-Cisd2-RNAi* (BDSC 33749) were obtained from the Bloomington Stock Center (BDSC). The RNAi control strains *UAS-vasa-RNAi* (VDRC46464) and *UAS-always-early-RNAi* (VDRC13673) were from the Vienna Drosophila Resource Center (VDRC). *Lifespan:* Fruit flies were provided with standard molasses-based food and accommodated in a climate chamber at a temperature of 25°C with a 12 h light and 12 h darkness schedule. The flies were given fresh food every two days and dead flies were scored. Each experiment consisted of four groups of 25 flies. Where indicated, fly food was prepared with deferiprone with a final concentration of 65 µM. *Climbing:* A total of four groups, each consisting of 25 flies per genotype per age, were tested in vials of a 2 cm diameter. The percentage of flies that were able to successfully traverse a height of 8 cm within 10 s was documented. The assay was always replicated at the same time of day. *Scoring for eclosed flies:* Fly food was prepared either with vehicle or with deferiprone (65 µM). A 3:1 ratio of female virgin flies to male flies (5-day old) were added and allowed to mate. These were then removed and the number of eclosing male flies per vial was quantified each day for three days. *Quantitative RT-PCR:* RNA extraction was carried out with the ZR RNA MiniPrep kit (ZYMO RESEARCH) and cDNA was synthesized from 10 ng/µl RNA using the High Capacity cDNA Reverse Transcription Kits (Life Tech). FastStart Universal SYBR Green Master (Rox) (Merck) was used for quantitative PCR (qPCR), with primers from Eurofins available on demand. The $2^{-\Delta\Delta Ct}$ (Ct, cycle of threshold) method was employed to calculate transcriptional levels, where ΔΔCt = ΔCt of experimental group – mean ΔCt of control groups. ΔCt = Ct (gene of interest) − Ct (RpL32/Rp49). RpL32/Rp49 served as housekeeping control. All flies used for these experiments were male. *Genomic DNA isolation and PCR:* Genomic DNA was extracted from flies using the Biozym gDNA Kit and PCR amplification performed to assess

the deletion in the Pink1 gene using the Q5 High-Fidelity DNA Polymerase (New England Biolabs). *Primer sequences:* Available on request.

GSH assay

Flies were mechanically lysed in PBS-EDTA in a tube containing 10% SSA, incubated on ice for 10 min and then centrifuged for 10 min at 4°C at 14000 rpm. The supernatant was added to a tube containing TEA:H_2O (1:1) while the pellet was left overnight at 37°C in 0.2N NaOH for protein concentration quantification. Samples were then pipetted alongside a standard. The assay mix containing DTNB, NADPH and glutathione reductase was added and absorbance was measured using a plate reader (Tecan) at 412 nm for 30 min. 5 flies were used per sample.

Dopamine quantification

Flies were anesthetized with CO_2 and heads removed while gently holding the flies with a tweezer. Heads were immediately put in a solution containing 200 µl 5% TCA, 300 µl RIPA buffer and 10 µl dopamine standards at 4°C. Ceramic beads were added and lysis was performed by gently shaking for 5 min. Lysates were cleared by centrifugation for 5 min at 13000 rpm twice. 200 µl of the supernatant was put in a fresh vial. Dopamine was determined via HPLC/MS/MS. 100 µL of 100 mM ammonium formate buffer (adjusted to pH 2.5 with formic acid) were added to 100 µL of the prepared extracts from fly heads in order to adjust pH in a HPLC-vial with insert. 50 µL of this solution were injected into the LC/MS/MS system consisting of an Agilent 1260 Infinity II Series HPLC pump (G7112B) with integrated degasser and an Agilent 1260 Autosampler (G7167A) connected to an AB Sciex 4500 tandem mass spectrometer. Chromatography was performed on a Phenomenex Kinetex F5 column (2.6 µM, 150 mm x 4.6 mm) using water (adjusted to pH 2.5) and acetonitrile as solvents A and B, respectively. Starting conditions were 5 % solvent B for 1 min, raised to 100 % B at 10 min, kept at 100 % B until 14 min and set back to 5 % B until 19 min and kept for another 5 min until 24 min. Flow rate was 0.3 ml/min. Tandem mass spectrometric determination was performed in ESI-negative mode using the specific ion transition 154,0 -> 137.0 for dopamine and 158.0 -> 140.9 for d4-dopamine as internal standard. We used an electrospray needle voltage of – 4500 V and nitrogen as a nebulizer and turbo heater gas (450°C) was set to a pressure of 65 psi. Nitrogen as curtain gas and collision gas was set to 10 instrument units, respectively. Calibration was performed in a mixture of 300 µL RIPA-buffer and 200 µL 5 % Trichloroacetic acid in water, spiked with dopamine concentrations ranging from 1 – 50 µg/L in HPLC-vials. 10 µL of the working solution of the internal standard (D_4-Dopamine, 1 mg/L in MeOH/HCl) were added to the standards, the vials were vortexed and centrifuged at 4.000 U/min (~ 3000 g). 100 µL of the supernatant was pipetted in a new HPLC vial with insert and 100 µL of 100 mM ammonium formate buffer (pH 2.5) were added. 50 µL of this solution was injected into the LC/MS/MS-system as described. As dopamine is not stable under neutral/basic conditions, the spiking solutions of dopamine (1 mg/L and 100 µg/L) were freshly prepared daily from the stock solution (1 g/L in MeOH/HCl) in 0.1% $HCl_{konz.}$ in water.

Iron quantification

Iron redox speciation in fly lysates was carried out using capillary electrophoresis (CE) coupled with inductively coupled plasma mass spectrometry (ICP-MS), referred to as CE-ICP-MS. To ensure interference-free monitoring of iron isotopes, dynamic reaction cell (DRC) technology employing NH3 as the DRC gas was utilized. A "PrinCe 706" CE system (PrinCe Technologies B.V., Emmen, Netherlands) was employed for the separation process, applying a voltage of +20 kV. The temperature settings for both the sample/buffer tray and

capillary were maintained at 20°C. An uncoated capillary (100 cm × 50 µm ID; CS-Chromatographie Service GmbH, Langerwehe, Germany) was used for interfacing with ICP–DRC-MS. The CE-ICP-MS interface enabled electrical connection while preventing suction flow by operating in self-aspiration mode (Michalke *et al*, 2019). The electrolytes used included 10% HCl as the leading electrolyte, 0.05 mM HCl as the terminating electrolyte, and 50 mM HCl as the background electrolyte. The Fe^{2+}/Fe^{3+} ratio was determined based on quantified concentrations of Fe species. An uncoated capillary (CS-Chromatographie Service GmbH, Langerwehe, Germany) measuring 85 cm in length with a 50 µm internal diameter was employed, connecting the CE system to the ICP-MS, served as the element-selective detector. A "NexIon 300-D" ICP-DRC-MS system (Perkin Elmer, Rodgau-Jügesheim, Germany) served as the element-selective detector for iron electropherograms. Isotopes ^{56}Fe and ^{57}Fe were measured in dynamic reaction cell (DRC) mode using ammonia as the DRC gas (0.58 ml NH3/min). The RF power was set to 1250 W, and the plasma gas flow was 16 L Ar/min. The nebulizer gas flow rate at the CE-ICP-DRC-MS interface was optimized to 0.98 L Ar/min. Electropherograms were analyzed using PeakfitTM software (Systat, Inpixon GmbH Office, Düsseldorf, Germany). To assess iron recovery accuracy, total iron content was determined using ICP-sector field mass spectrometry (ICP-sf-MS). The ICP-sf-MS ("ELEMENT 2", Thermo Scientific, Bremen, Germany) settings included a radio frequency power of 1260 W, a plasma gas flow of 16 L Ar/min, an auxiliary gas flow of 0.85 L Ar/min, a nebulizer gas flow of 1.085 L Ar/min, and a dwell time of 300 ms. Quantified iron species from CE-ICP-DRC-MS were compared to total iron content (set at 100%), yielding values ranging between 92% and 110%.

Transmission electron microscopy

Fly thoraxes were isolated and fixed in a buffer containing (Caco-buffer (0.2M), 25% Glutaraldehyde (GA), and 15% Paraformaldehyde (PFA)). After fixation, tissues were washed in a wash buffer (0.2M Caco-buffer diluted 1:1 with ddH_2O) and incubated with 2% Osmium in 0.2M buffer. Tissues were washed again and dehydrated in ascending ethanol series 30% to 70% then left overnight at 4°C. The next day, the samples were dehydrated further in 80%, 90%, 95%, and 100% ethanol solutions then washed with propylenoxide and left overnight in a 1:1 dilution of resin: proyleneoxide. Samples were moved the next day to just resin. The last day, flies were placed into a special mold with resin and left in an oven for two days. Samples were then cut and contrasted. Images were acquired with a Tnecnai 12 Transmission electron microscope.

Statistical analysis

Statistical analysis was performed using Graphpad prism. Data were tested for normality using the Shapiro-Wilk test. Two parametric samples were compared using the student's t test, two nonparametric samples using the Mann Whitney test, two normalized parametric samples using the one-sided t test, two non-parametric samples using the Wilcoxon signed-rank test. More than two parametric samples were compared using one-way or two-way ANOVA and nonparametric samples using the Kruskal-Wallis test followed by the respective post-hoc tests.

Declarations

Ethics approval and consent to participate

Induced pluripotent stem cells (iPSCs) from two PD patients carrying the p.Q456X mutation in PINK1 were obtained from the University of Lübeck. Written informed consent is available at the University of Lübeck.

Consent for publication

Not applicable

Availability of data and materials

All data generated or analyzed during this study are included in this published article (and its supplementary information files).

Competing interests

The authors declare that they have no competing interests

Funding

This work was funded by the Deutsche Forschungsgemeinschaft to AM (ME1922/17-1). GA is supported by the Luxembourg National Research Fund (C21/BM/15850547/PINK1-DiaPDs).

Authors' contributions

SB, TB, CW, MA, LCR, TS, IER, BM, GA, LZ performed experiments. LZ, VV, PZ, RK and AM supervised experiments. AM analyzed data and interpreted results. AM wrote the manuscript.

Acknowledgements

We thank Christine Klein and Philipp Seibler (University of Lübeck, Germany) who kindly shared the human iPSC lines from PD patients carrying the PINK1 p.Q456X mutation, and Jens Schwamborn and Javier Jarazo (LCSB, University of Luxembourg, Luxembourg) for providing the corresponding gene-corrected controls. We also thank Marion Silies, JGU Mainz, for providing lab space and helpful discussions. This work contains data from the medical theses of Timo Baumann, Majd Abusaada and Christopher Weber.

References

Allen GFG, Toth R, James J & Ganley IG (2013) Loss of iron triggers PINK1/Parkin-independent mitophagy. *EMBO Rep* 14: 1127–1135

Antico O, Ordureau A, Stevens M, Singh F, Nirujogi RS, Gierlinski M, Barini E, Rickwood ML, Prescott A, Toth R, *et al* (2021) Global ubiquitylation analysis of mitochondria in primary neurons identifies endogenous Parkin targets following activation of PINK1. *Sci Adv* 7: eabj0722

Bus C, Zizmare L, Feldkaemper M, Geisler S, Zarani M, Schaedler A, Klose F, Admard J, Mageean CJ, Arena G, *et al* (2020) Human Dopaminergic Neurons Lacking PINK1 Exhibit Disrupted Dopamine Metabolism Related to Vitamin B6 Co-Factors. *iScience* 23: 101797

Camponeschi F, Ciofi-Baffoni S & Banci L (2017) Anamorsin/Ndor1 Complex Reduces [2Fe-2S]-MitoNEET via a Transient Protein-Protein Interaction. *J Am Chem Soc* 139: 9479–9482

Chan NC, Salazar AM, Pham AH, Sweredoski MJ, Kolawa NJ, Graham RLJ, Hess S & Chan DC (2011) Broad activation of the ubiquitin-proteasome system by Parkin is critical for mitophagy. *Hum Mol Genet* 20: 1726–1737

Chen OS, Schalinske KL & Eisenstein RS (1997) Dietary iron intake modulates the activity of iron regulatory proteins and the abundance of ferritin and mitochondrial aconitase in rat liver. *J Nutr* 127: 238–248

Chen P-L, Huang K-T, Cheng C-Y, Li J-C, Chan H-Y, Lin T-Y, Su MP, Yang W-Y, Chang HC, Wang H-D, *et al* (2020) Vesicular transport mediates the uptake of cytoplasmic proteins into mitochondria in Drosophila melanogaster. *Nat Commun* 11: 2592

Clark IE, Dodson MW, Jiang C, Cao JH, Huh JR, Seol JH, Yoo SJ, Hay BA & Guo M (2006) Drosophila pink1 is required for mitochondrial function and interacts genetically with parkin. *Nature* 441: 1162–1166

Cunningham CN, Baughman JM, Phu L, Tea JS, Yu C, Coons M, Kirkpatrick DS, Bingol B & Corn JE (2015) USP30 and parkin homeostatically regulate atypical ubiquitin chains on mitochondria. *Nat Cell Biol* 17: 160–169

Dexter DT, Wells FR, Agid F, Agid Y, Lees AJ, Jenner P & Marsden CD (1987) Increased nigral iron content in postmortem parkinsonian brain. *Lancet* 2: 1219–1220

Dixon AS, Schwinn MK, Hall MP, Zimmerman K, Otto P, Lubben TH, Butler BL, Binkowski BF, Machleidt T, Kirkland TA, *et al* (2016) NanoLuc Complementation Reporter Optimized for Accurate Measurement of Protein Interactions in Cells. *ACS Chem Biol* 11: 400–408

Esposito G, Vos M, Vilain S, Swerts J, De Sousa Valadas J, Van Meensel S, Schaap O & Verstreken P (2013) Aconitase causes iron toxicity in Drosophila pink1 mutants. *PLoS Genet* 9: e1003478

Ferecatu I, Gonçalves S, Golinelli-Cohen M-P, Clémancey M, Martelli A, Riquier S, Guittet E, Latour J-M, Puccio H, Drapier J-C, *et al* (2014) The diabetes drug target MitoNEET governs a novel trafficking pathway to rebuild an Fe-S cluster into cytosolic aconitase/iron regulatory protein 1. *J Biol Chem* 289: 28070–28086

Furihata T, Takada S, Kakutani N, Maekawa S, Tsuda M, Matsumoto J, Mizushima W, Fukushima A, Yokota T, Enzan N, *et al* (2021) Cardiac-specific loss of mitoNEET expression is linked with age-related heart failure. *Commun Biol* 4: 138

Galy B, Ferring-Appel D, Sauer SW, Kaden S, Lyoumi S, Puy H, Kölker S, Gröne H-J & Hentze MW (2010) Iron regulatory proteins secure mitochondrial iron sufficiency and function. *Cell Metab* 12: 194–201

Gautier CA, Kitada T & Shen J (2008) Loss of PINK1 causes mitochondrial functional defects and increased sensitivity to oxidative stress. *Proc Natl Acad Sci U S A* 105: 11364–11369

Geldenhuys WJ, Benkovic SA, Lin L, Yonutas HM, Crish SD, Sullivan PG, Darvesh AS, Brown CM & Richardson JR (2017) MitoNEET (CISD1) Knockout Mice Show Signs of Striatal Mitochondrial Dysfunction and a Parkinson's Disease Phenotype. *ACS Chem Neurosci* 8: 2759–2765

Geldenhuys WJ, Funk MO, Barnes KF & Carroll RT (2010) Structure-based design of a thiazolidinedione which targets the mitochondrial protein mitoNEET. *Bioorg Med Chem Lett* 20: 819–823

Greene JC, Whitworth AJ, Andrews LA, Parker TJ & Pallanck LJ (2005) Genetic and genomic studies of Drosophila parkin mutants implicate oxidative stress and innate immune responses in pathogenesis. *Hum Mol Genet* 14: 799–811

Haile DJ, Rouault TA, Harford JB, Kennedy MC, Blondin GA, Beinert H & Klausner RD (1992a) Cellular regulation of the iron-responsive element binding protein: disassembly of the cubane iron-sulfur cluster results in high-affinity RNA binding. *Proc Natl Acad Sci U S A* 89: 11735–11739

Haile DJ, Rouault TA, Tang CK, Chin J, Harford JB & Klausner RD (1992b) Reciprocal control of RNA-binding and aconitase activity in the regulation of the iron-responsive element binding protein: role of the iron-sulfur cluster. *Proc Natl Acad Sci U S A* 89: 7536–7540

Ham SJ, Yoo H, Woo D, Lee DH, Park K-S & Chung J (2023) PINK1 and Parkin regulate IP3R-mediated ER calcium release. *Nat Commun* 14: 5202

Hirsch EC, Brandel JP, Galle P, Javoy-Agid F & Agid Y (1991) Iron and aluminum increase in the substantia nigra of patients with Parkinson's disease: an X-ray microanalysis. *J Neurochem* 56: 446–451

Hou X, Liu R, Ross S, Smart EJ, Zhu H & Gong W (2007) Crystallographic studies of human MitoNEET. *J Biol Chem* 282: 33242–33246

Huynh N, Ou Q, Cox P, Lill R & King-Jones K (2019) Glycogen branching enzyme controls cellular iron homeostasis via Iron Regulatory Protein 1 and mitoNEET. *Nat Commun* 10: 5463

Jarazo J, Barmpa K, Modamio J, Saraiva C, Sabaté-Soler S, Rosety I, Griesbeck A, Skwirblies F, Zaffaroni G, Smits LM, *et al* (2022) Parkinson's Disease Phenotypes in Patient Neuronal Cultures and Brain Organoids Improved by 2-Hydroxypropyl-β-Cyclodextrin Treatment. *Mov Disord* 37: 80–94

Jones MA, Amr S, Ferebee A, Huynh P, Rosenfeld JA, Miles MF, Davies AG, Korey CA, Warrick JM, Shiang R, *et al* (2014) Genetic studies in Drosophila and humans support a model for the concerted function of CISD2, PPT1 and CLN3 in disease. *Biol Open* 3: 342–352

Karmi O, Marjault H-B, Bai F, Roy S, Sohn Y-S, Darash Yahana M, Morcos F, Ioannidis K, Nahmias Y, Jennings PA, *et al* (2022) A VDAC1-mediated NEET protein chain transfers [2Fe-2S] clusters between the mitochondria and the cytosol and impacts mitochondrial dynamics. *Proc Natl Acad Sci U S A* 119

Key J, Sen NE, Arsović A, Krämer S, Hülse R, Khan NN, Meierhofer D, Gispert S, Koepf G & Auburger G (2020) Systematic Surveys of Iron Homeostasis Mechanisms Reveal Ferritin Superfamily and Nucleotide Surveillance Regulation to be Modified by PINK1 Absence. *Cells* 9

Kim HY, LaVaute T, Iwai K, Klausner RD & Rouault TA (1996) Identification of a conserved and functional iron-responsive element in the 5'-untranslated region of mammalian mitochondrial aconitase. *J Biol Chem* 271: 24226–24230

LaVaute T, Smith S, Cooperman S, Iwai K, Land W, Meyron-Holtz E, Drake SK, Miller G, Abu-Asab M, Tsokos M, *et al* (2001) Targeted deletion of the gene encoding iron regulatory protein-2 causes misregulation of iron metabolism and neurodegenerative disease in mice. *Nat Genet* 27: 209–214

Lazarou M, Narendra DP, Jin SM, Tekle E, Banerjee S & Youle RJ (2013) PINK1 drives Parkin self-association and HECT-like E3 activity upstream of mitochondrial binding. *J Cell Biol* 200: 163–172

Lee JJ, Sanchez-Martinez A, Martinez Zarate A, Benincá C, Mayor U, Clague MJ & Whitworth AJ (2018) Basal mitophagy is widespread in Drosophila but minimally affected by loss of Pink1 or parkin. *J Cell Biol* 217: 1613–1622

Lee S, Lee S, Lee S-J & Chung SW (2022a) Inhibition of mitoNEET induces

Pink1-Parkin-mediated mitophagy. *BMB Rep* 55: 354–359

Lee S, Seok BG, Lee S-J & Chung SW (2022b) Inhibition of mitoNEET attenuates LPS-induced inflammation and oxidative stress. *Cell Death Dis* 13: 127

Lin J, Zhou T, Ye K & Wang J (2007) Crystal structure of human mitoNEET reveals distinct groups of iron sulfur proteins. *Proc Natl Acad Sci U S A* 104: 14640–14645

Lozinsky OV, Lushchak OV, Kryshchuk NI, Shchypanska NY, Riabkina AH, Skarbek SV, Maksymiv IV, Storey JM, Storey KB & Lushchak VI (2013) S-nitrosoglutathione-induced toxicity in Drosophila melanogaster: Delayed pupation and induced mild oxidative/nitrosative stress in eclosed flies. *Comp Biochem Physiol A Mol Integr Physiol* 164: 162–170

Ma L, Gholam Azad M, Dharmasivam M, Richardson V, Quinn RJ, Feng Y, Pountney DL, Tonissen KF, Mellick GD, Yanatori I, *et al* (2021) Parkinson's disease: Alterations in iron and redox biology as a key to unlock therapeutic strategies. *Redox Biol* 41: 101896

Martinez A, Lectez B, Ramirez J, Popp O, Sutherland JD, Urbé S, Dittmar G, Clague MJ & Mayor U (2017) Quantitative proteomic analysis of Parkin substrates in Drosophila neurons. *Mol Neurodegener* 12: 29

Martinez A, Sanchez-Martinez A, Pickering JT, Twyning MJ, Terriente-Felix A, Chen P-L, Chen C-H & Whitworth AJ (2023) Mitochondrial CISD1/Cisd accumulation blocks mitophagy and genetic or pharmacological inhibition rescues neurodegenerative phenotypes in Pink1/parkin models. *bioRxiv*: 2023.05.14.540700

McWilliams TG, Barini E, Pohjolan-Pirhonen R, Brooks SP, Singh F, Burel S, Balk K, Kumar A, Montava-Garriga L, Prescott AR, *et al* (2018) Phosphorylation of Parkin at serine 65 is essential for its activation in vivo. *Open Biol* 8

Michalke B, Willkommen D & Venkataramani V (2019) Iron Redox Speciation Analysis Using Capillary Electrophoresis Coupled to Inductively Coupled Plasma Mass Spectrometry (CE-ICP-MS). *Front Chem* 7: 136

Mittler R, Darash-Yahana M, Sohn YS, Bai F, Song L, Cabantchik IZ, Jennings PA, Onuchic JN & Nechushtai R (2019) NEET Proteins: A New Link Between Iron Metabolism, Reactive Oxygen Species, and Cancer. *Antioxid Redox Signal* 30: 1083–1095

Narendra DP, Wang C, Youle RJ & Walker JE (2013) PINK1 rendered temperature sensitive by disease-associated and engineered mutations. *Hum Mol Genet* 22: 2572–2589

Narendra D, Tanaka A, Suen D-F & Youle RJ (2008) Parkin is recruited selectively to impaired mitochondria and promotes their autophagy. *J Cell Biol* 183: 795–803

Narendra D, Walker JE & Youle R (2012) Mitochondrial quality control mediated by PINK1 and Parkin: links to parkinsonism. *Cold Spring Harb Perspect Biol* 4

Okatsu K, Iemura S-I, Koyano F, Go E, Kimura M, Natsume T, Tanaka K & Matsuda N (2012) Mitochondrial hexokinase HKI is a novel substrate of the Parkin ubiquitin ligase. *Biochem Biophys Res Commun* 428: 197–202

Paddock ML, Wiley SE, Axelrod HL, Cohen AE, Roy M, Abresch EC, Capraro D, Murphy AN, Nechushtai R, Dixon JE, *et al* (2007) MitoNEET is a uniquely folded 2Fe 2S outer mitochondrial membrane protein stabilized by pioglitazone. *Proc Natl Acad Sci U S A* 104: 14342–14347

Park J, Lee SB, Lee S, Kim Y, Song S, Kim S, Bae E, Kim J, Shong M, Kim J-M, *et al* (2006) Mitochondrial dysfunction in Drosophila PINK1 mutants is complemented by parkin. *Nature* 441: 1157–1161

Pickrell AM & Youle RJ (2015) The roles of PINK1, parkin, and mitochondrial fidelity in Parkinson's disease. *Neuron* 85: 257–273

Polyansky AA, Chugunov AO, Volynsky PE, Krylov NA, Nolde DE & Efremov RG (2014) PREDDIMER: a web server for prediction of transmembrane helical dimers. *Bioinformatics* 30: 889–890

Pyatigorskaya N, Sharman M, Corvol J-C, Valabregue R, Yahia-Cherif L, Poupon F, Cormier-Dequaire F, Siebner H, Klebe S, Vidailhet M, *et al* (2015) High nigral iron deposition in LRRK2 and Parkin mutation carriers using R2* relaxometry. *Mov Disord* 30: 1077–1084

Reinhardt P, Glatza M, Hemmer K, Tsytsyura Y, Thiel CS, Höing S, Moritz S, Parga JA, Wagner L, Bruder JM, *et al* (2013) Derivation and expansion using only small molecules of human neural progenitors for neurodegenerative disease modeling. *PLoS One* 8: e59252

Rouault TA & Maio N (2017) Biogenesis and functions of mammalian iron-sulfur proteins in the regulation of iron homeostasis and pivotal metabolic pathways. *J Biol Chem* 292: 12744–12753

Saralkar P, Mdzinarishvili A, Arsiwala TA, Lee Y-K, Sullivan PG, Pinti MV, Hollander JM, Kelley EE, Ren X, Hu H, *et al* (2021) The Mitochondrial mitoNEET Ligand NL-1 Is Protective in a Murine Model of Transient Cerebral Ischemic Stroke. *Pharm Res* 38: 803–817

Sarraf SA, Raman M, Guarani-Pereira V, Sowa ME, Huttlin EL, Gygi SP & Harper JW (2013) Landscape of the PARKIN-dependent ubiquitylome in response to mitochondrial depolarization. *Nature* 496: 372–376

Shulman JM, De Jager PL & Feany MB (2011) Parkinson's disease: genetics and pathogenesis. *Annu Rev Pathol* 6: 193–222

Tan G, Liu D, Pan F, Zhao J, Li T, Ma Y, Shen B & Lyu J (2016) His-87 ligand in mitoNEET is crucial for the transfer of iron sulfur clusters from mitochondria to cytosolic aconitase. *Biochem Biophys Res Commun* 470: 226–232

Vernay A, Marchetti A, Sabra A, Jauslin TN, Rosselin M, Scherer PE, Demaurex N, Orci L & Cosson P (2017) MitoNEET-dependent formation of intermitochondrial junctions. *Proc Natl Acad Sci U S A* 114: 8277–8282

Wang C-H, Chen Y-F, Wu C-Y, Wu P-C, Huang Y-L, Kao C-H, Lin C-H, Kao L-S, Tsai T-F & Wei Y-H (2014) Cisd2 modulates the differentiation and functioning of adipocytes by regulating intracellular Ca2+ homeostasis. *Hum Mol Genet* 23: 4770–4785

Wan Z, Xu J, Huang Y, Zhai Y, Ma Z, Zhou B & Cao Z (2020) Elevating bioavailable iron levels in mitochondria suppresses the defective phenotypes caused by PINK1 loss-of-function in Drosophila melanogaster. *Biochem Biophys Res Commun* 532: 285–291

Whitworth AJ, Theodore DA, Greene JC, Benes H, Wes PD & Pallanck LJ (2005) Increased glutathione S-transferase activity rescues dopaminergic neuron loss in a Drosophila model of Parkinson's disease. *Proc Natl Acad Sci U S A* 102: 8024–8029

Wiley SE, Murphy AN, Ross SA, van der Geer P & Dixon JE (2007a) MitoNEET is an iron-containing outer mitochondrial membrane protein that regulates oxidative capacity. *Proc Natl Acad Sci U S A* 104: 5318–5323

Wiley SE, Paddock ML, Abresch EC, Gross L, van der Geer P, Nechushtai R, Murphy AN, Jennings PA & Dixon JE (2007b) The outer mitochondrial membrane protein mitoNEET contains a novel redox-active 2Fe-2S cluster. *J Biol Chem* 282: 23745–23749

Yonutas HM, Hubbard WB, Pandya JD, Vekaria HJ, Geldenhuys WJ & Sullivan PG (2020) Bioenergetic restoration and neuroprotection after therapeutic targeting of mitoNEET: New mechanism of pioglitazone following traumatic brain injury. *Exp Neurol* 327: 113243

Youle RJ & Narendra DP (2011) Mechanisms of mitophagy. *Nat Rev Mol Cell Biol* 12: 9–14

Supplementary figures

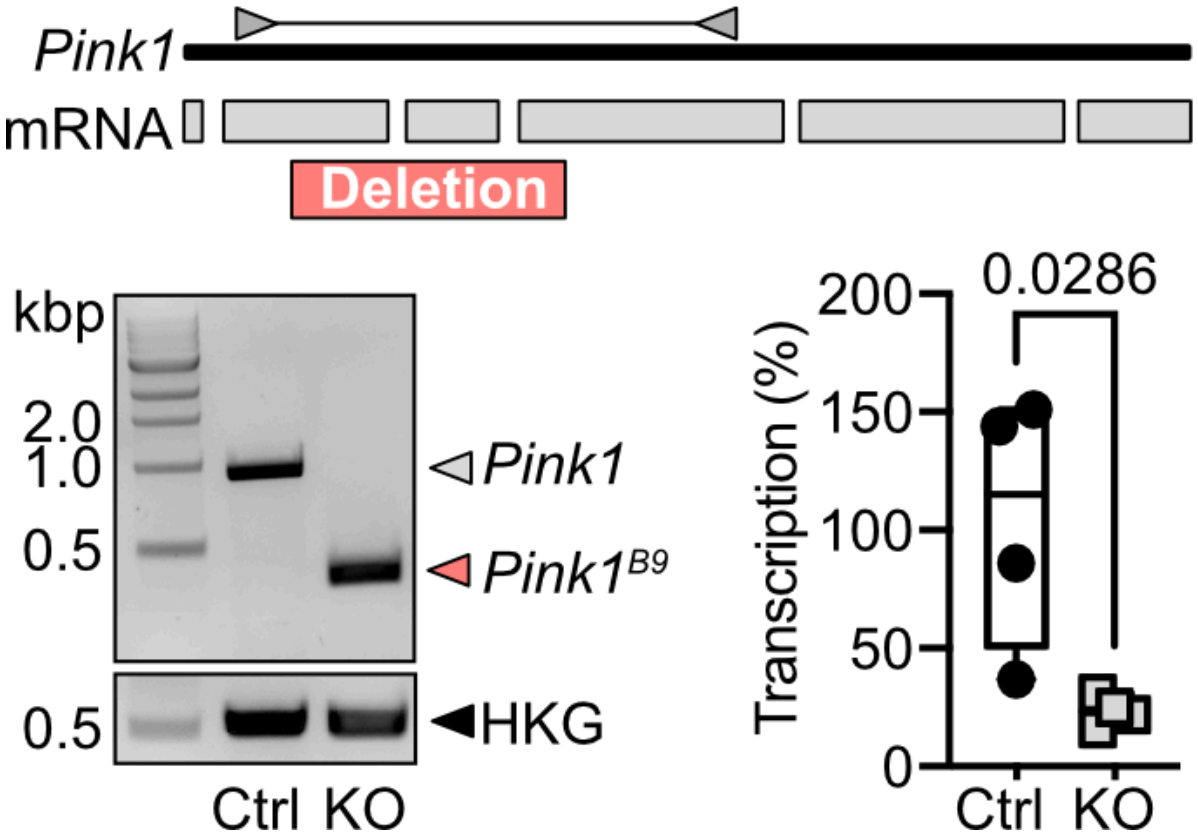

Supplementary Figure 1 Validation of Pink1 Knockout flies. Pink1 genomic organization with mRNA/exons represented as light gray boxes. A 571 nt deletion extending from the 2nd to 4th exon is shown in orange. Validation PCR, using indicated primers (dark gray triangles), results in a 917 nt product for wild-type Pink1 and 246 nt for knockout Pink1. mRNA levels were assessed using qPCR with primers at the 4th and 5th exon junction. HKG: Housekeeping gene, Rp49; Ctrl: Control flies, w^{1118}; KO: Pink1 mutant flies ($Pink1^{B9}$).

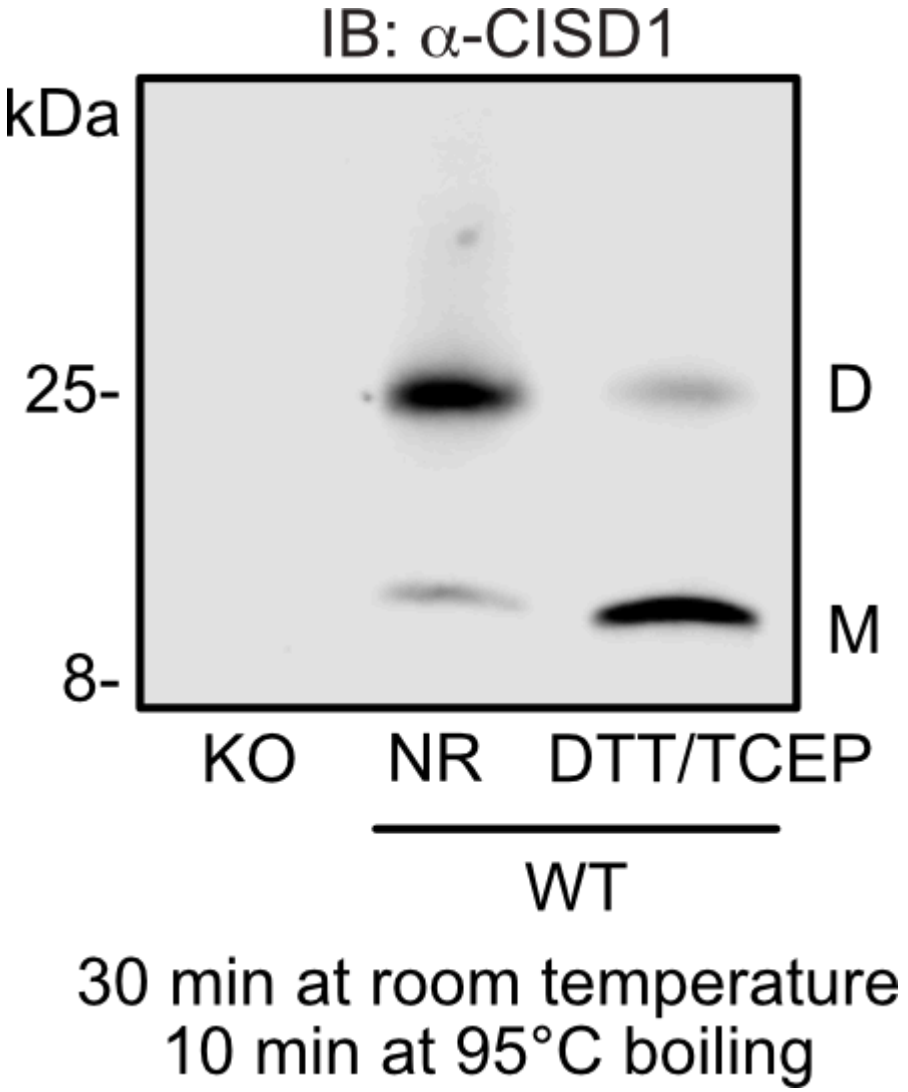

Supplementary Figure 2 Conditions that result in reduction of Cisd. Immunoblot analysis of Cisd expression in w^{1118} flies Samples were exposed to a non-reducing buffer (NR) or reducing buffer containing 100 mM DTT and 50 mM TCEP. Cisd KO lysates served as negative control for the Cisd bands. Actin served as loading control, size is indicated. (M) Cisd monomers and (D) dimers.

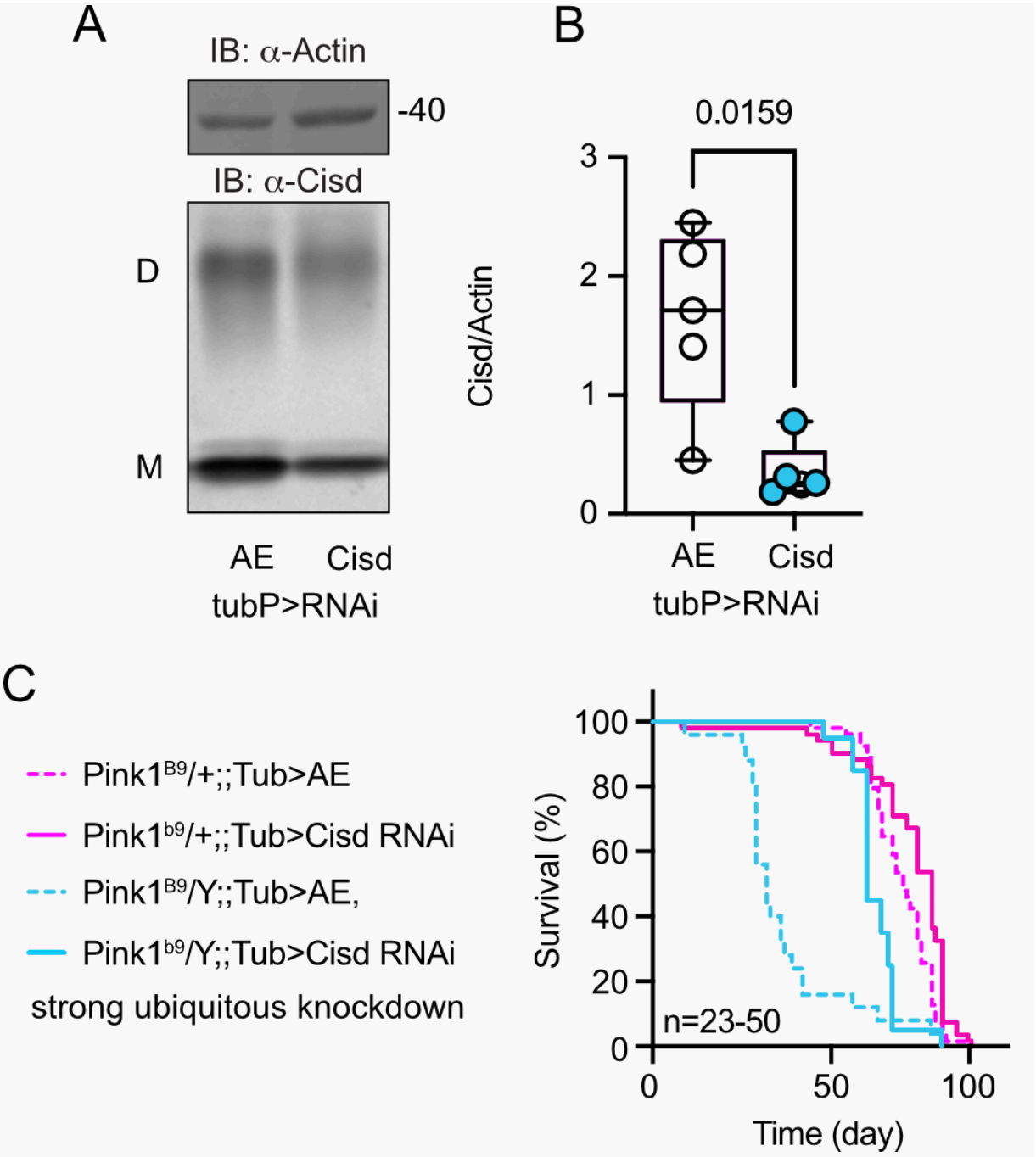

Supplementary Figure 3 RNAi-mediated knockdown of Cisd protects against Pink1 loss of function. a. Immunoblot demonstrating Cisd knockdown, always-early RNAi served as control and actin as loading control. Note the presence of Cisd monomers (M) and dimers (D) even in reducing gels. **b.** Survival of hemizygous *Pink1*^{B9} on standard food. Fresh food was supplied and the number of dead flies was scored every two days, n is indicated.

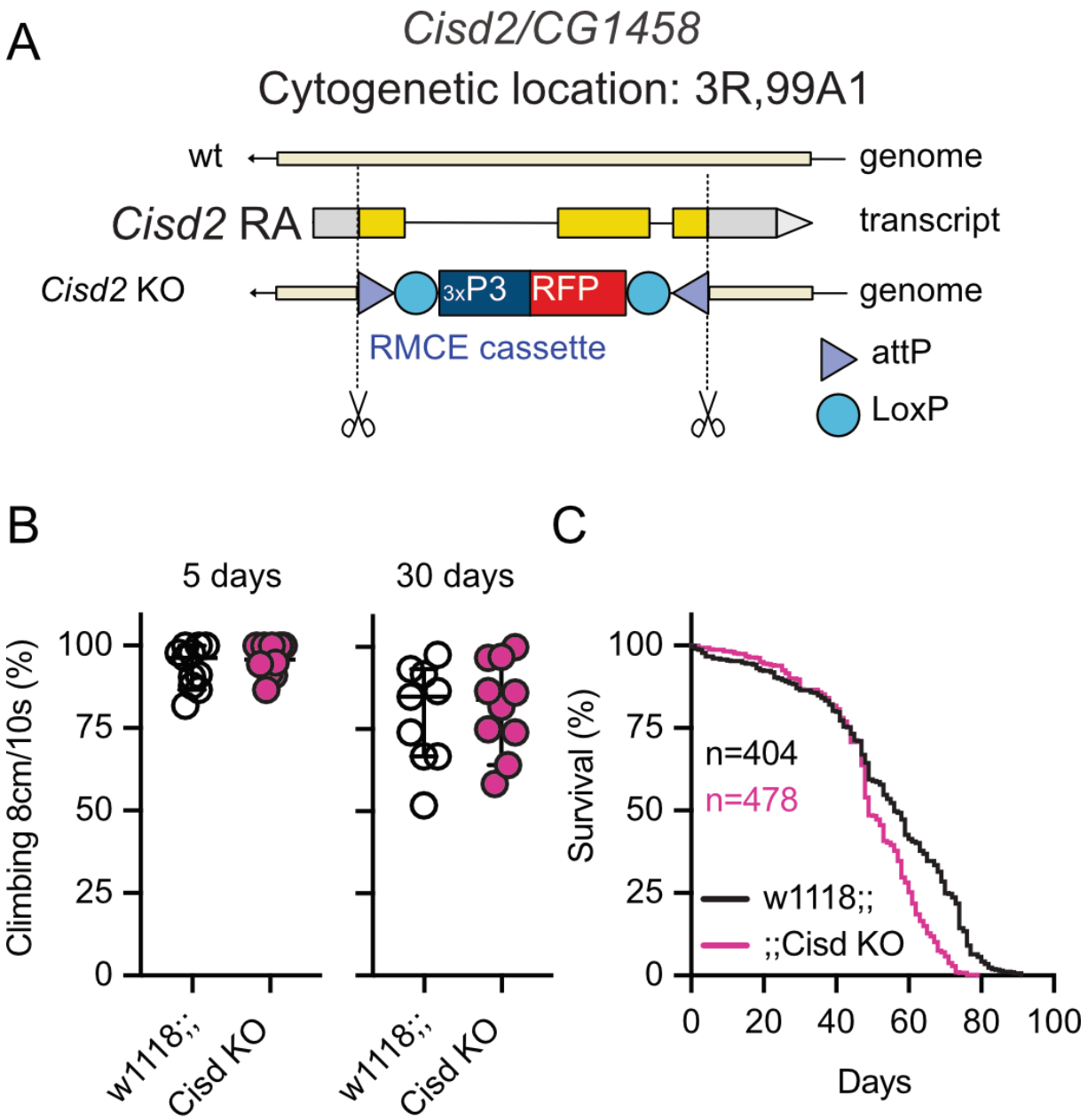

Supplementary Figure 4 Phenotypes of Cisd knockout flies. a. Scheme depicting the construction of Cisd knockout flies. **b.** Climbing ability assessment. Each dot represents the percentage of a group of 25 flies that climbed more than 8 cm within 10 s. **c.** Survival of wildtype (w1118) and Cisd KO flies on standard food. Fresh food was supplied and the number of dead flies was scored every two days, n is indicated.

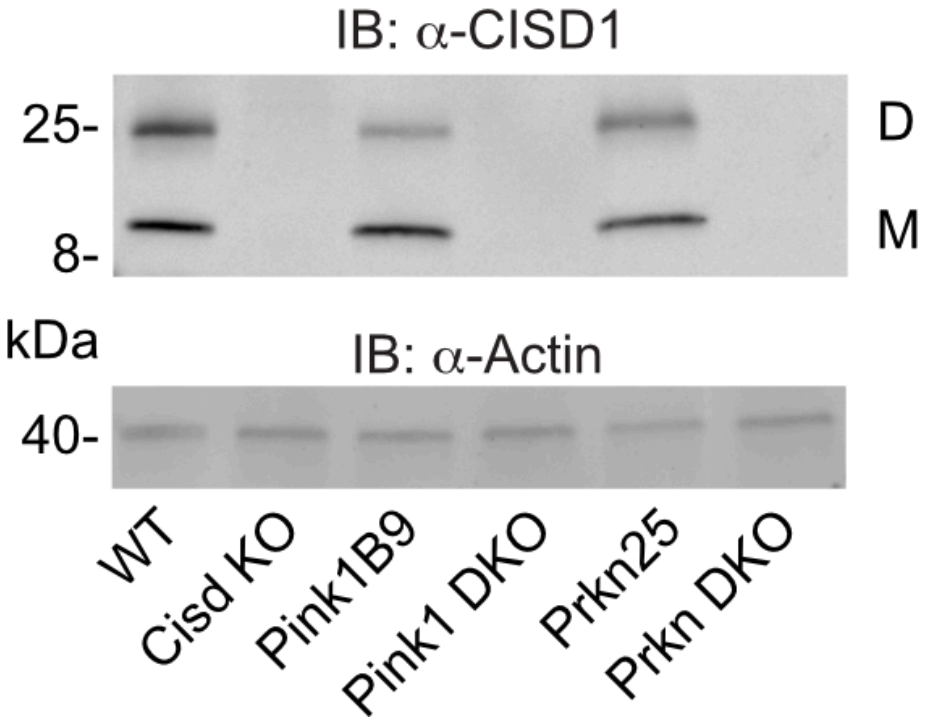

Supplementary Figure 5 Double-knockout flies lack Cisd protein expression. Immunoblot analysis of Cisd abundance in the indicated fly strains 3 days after eclosion. Actin served as loading control, size is indicated. (M) Cisd monomers and (D) dimers.

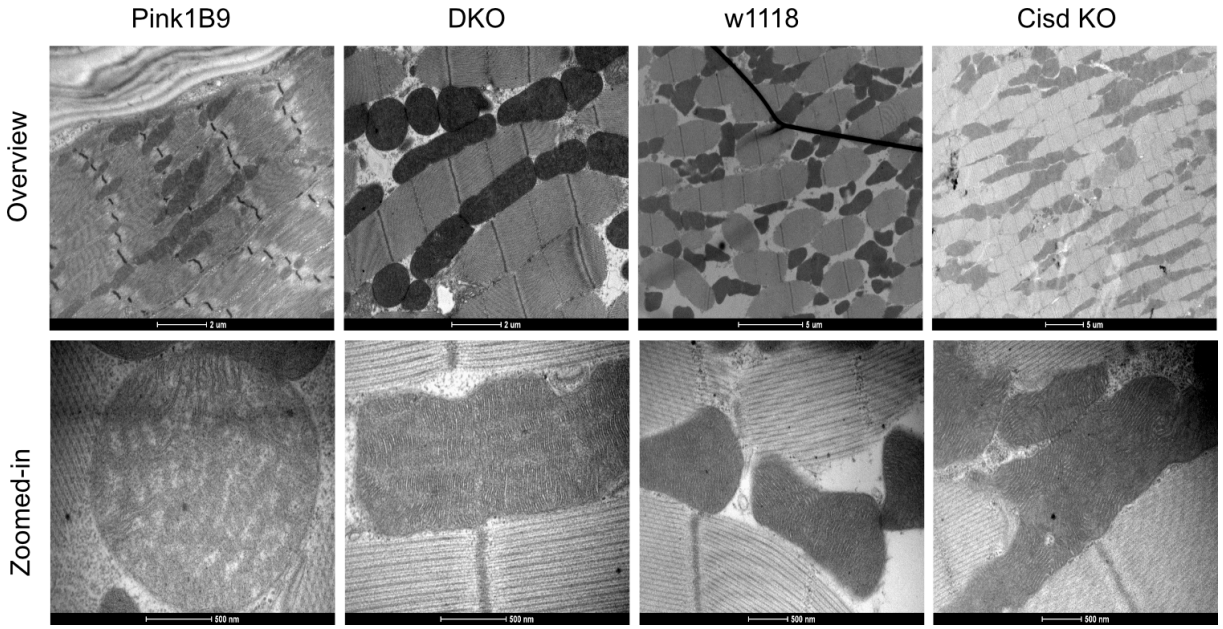

Supplementary Figure 6 Exemplary transmission electron microscopy pictures. Representative transmission electron microscopy of flight muscle morphology from the indicated fly strains. Scale bar as indicated.